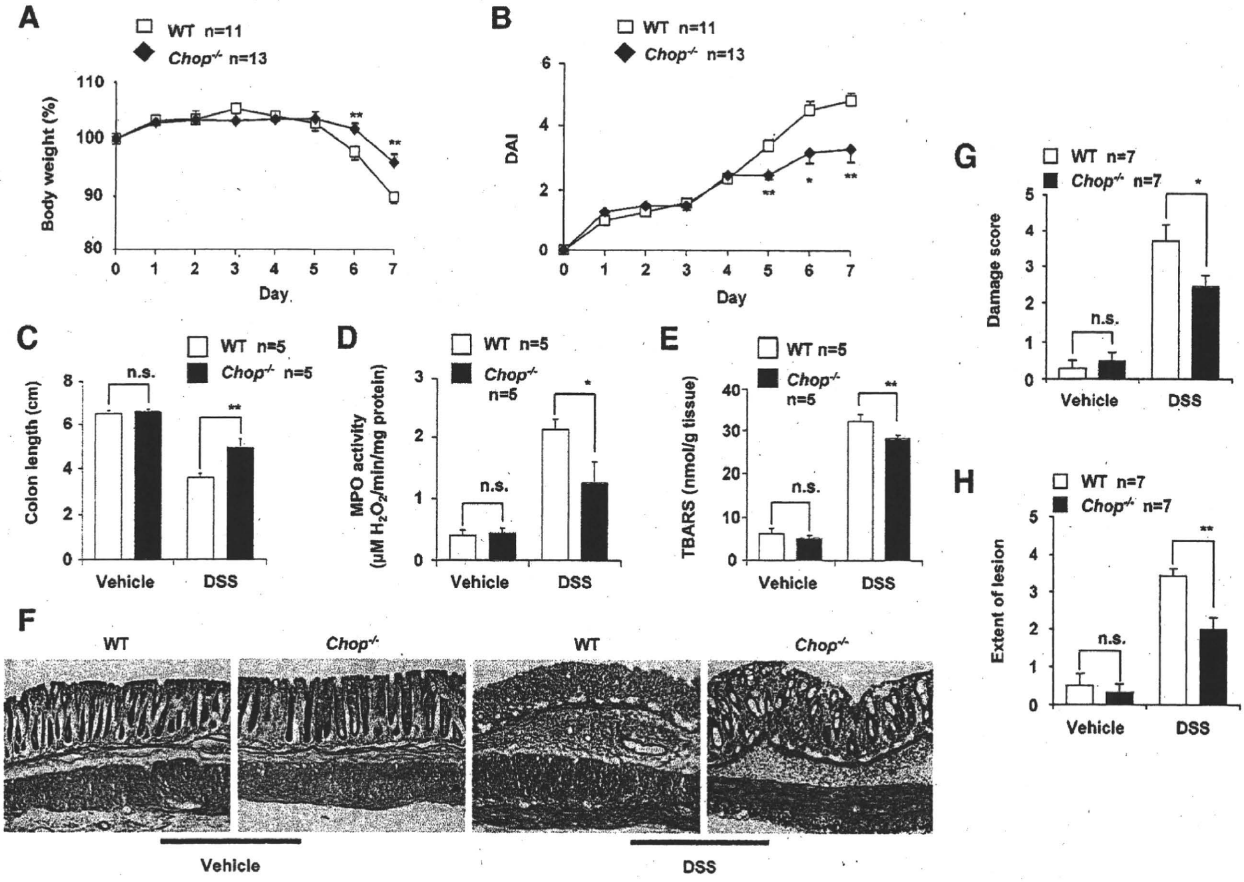

Figure 1. Development of DSS-induced colitis in CHOP-null mice and WT mice. CHOP-null mice (*Chop*$^{-/-}$) and WT mice were treated with or without 3% DSS for 7 days. Body weight (**A**) and DAI (**B**) were measured daily. After 7 days, length of colon (**C**), colonic MPO activity (**D**), and colonic TBARS (**E**) were determined as described in the Materials and Methods. **G** and **H:** After 7 days, sections of colonic tissues were prepared and subjected to histological examination (H&E staining) and the damage score and extent of lesion for seven independent sections were determined. **F:** One of the sections is shown. Values are mean ± SEM (n = 5 to 13). $^{**}P < 0.01$; $^{*}P < 0.05$; n.s., not significant.

phometric measure for the degree of inflammation, was less severe in CHOP-null mice than in the WT mice (Figure 1C). Colonic MPO activity, an indicator of infiltration of leukocytes, was lower in DSS-administered CHOP-null mice than in the WT mice (Figure 1D). Colonic TBARS, an index of lipid peroxidation associated with inflammation, was also lower in DSS-administered CHOP-null mice than in the WT mice (Figure 1E). Absence of the *Chop* gene did not affect the background levels of these indices (colon length, colonic MPO activity, and colonic TBARS) (Figure 1, C–E). Figure 1F shows results of histological analyses of colonic tissues prepared from DSS-administered and control CHOP-null mice and WT mice. Crypt loss and infiltration of leukocytes were more apparent in sections from DSS-administered WT mice than those from CHOP-null mice. Histological score analysis (damage score and extent of lesion) revealed that the histological differences between DSS-administered CHOP-null mice and the WT mice were statistically significant (Figure 1, G and H). Results in Figure 1 show that CHOP-null mice are more resistant to DSS-induced colitis than the WT mice.

We examined the effect of DSS administration on expression of CHOP and GRP78 in the intestine at both mRNA and protein levels. Analysis by real-time RT-PCR revealed that the mRNA expression of *Chop* in colonic tissues was induced by the DSS administration in the WT mice and that the *Chop* mRNA was not expressed in CHOP-null mice (Figure 2A). The mRNA expression of *Grp78* was also induced by DSS administration (Figure 2A), suggesting that the ER stress response is induced simultaneously with development of DSS-induced colitis. Results in Figure 2A also suggest that CHOP positively regulates the mRNA expression of *Grp78* in the intestine.

Immunohistochemical and immunoblotting analyses demonstrated that DSS administration increases the level of CHOP in colonic tissues in the WT mice but not in CHOP-null mice (Figure 2, B and D). CHOP expression was localized in nuclei, being consistent that CHOP is a transcription factor. We also found that DSS administration increases the level of GRP78 in colonic tissues in WT mice and that this increase was not so clearcut in CHOP-null mice (Figure 2, C and D).

We also examined the effect of a deficiency in CHOP on the development of TNBS-induced colitis. As shown in Figure 3A, a TNBS (3 mg/kg)-dependent decrease in body weight was less apparent in CHOP-null mice than in WT mice. Administration of a higher dose of TNBS (8 mg/kg) caused the death of some mice, with the survival rate of CHOP-null mice being much higher than that of

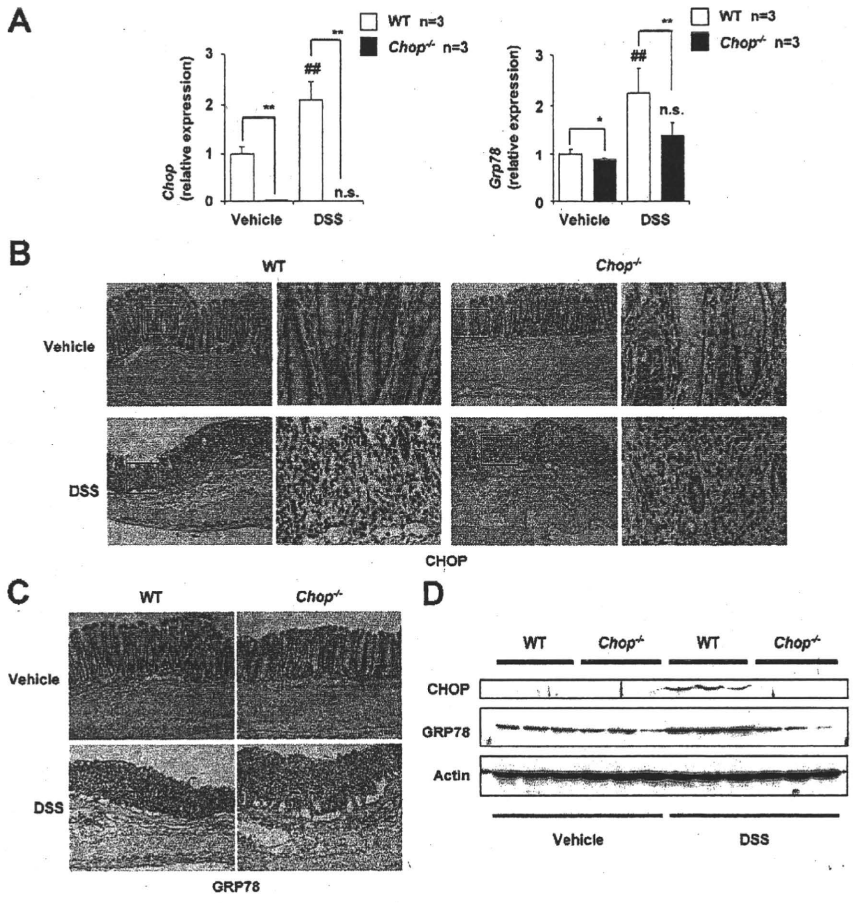

Figure 2. Expression of CHOP and GRP78 in colonic tissues of CHOP-null mice and WT mice. DSS was administered to CHOP-null mice (*Chop*$^{-/-}$) and WT mice, as described in the legend of Figure 1. Colonic tissues were removed and total RNA was extracted. Samples were subjected to real-time RT-PCR, using a specific primer set for *Chop* or *Grp78*. Values were normalized to *Gapdh*, expressed relative to the control sample (ie, WT mice without DSS treatment), and given as the mean ± SEM ($n = 4$). **A:** ** or **$P < 0.01$; *$P < 0.05$; n.s., not significant. Sections of colonic tissues were prepared and subjected to immunohistochemical analysis with an antibody against CHOP (**B**) or GRP78 (**C**). **B:** The **right panel** in each column is a ×4 magnified image of the boxed area defined in the **left panel**. **D:** Total protein was extracted from colonic tissues and analyzed by immunoblotting with an antibody against CHOP, GRP78, or actin.

WT mice (Figure 3B). Histological analysis of colonic tissues revealed that TNBS-dependent intestinal mucosal damage was more severe in the WT mice than in CHOP-null mice (Figure 3, C–E). We also found that this TNBS (3 mg/kg) administration up-regulated the mRNA expression of *Chop* and *Grp78* in the intestine (data not shown).

Analysis of the mRNA Expression of Various Genes in DSS-Administered CHOP-Null Mice and WT Mice

To obtain a better understanding of the molecular mechanism governing CHOP-dependent exacerbation of DSS-induced colitis, we compared the mRNA expression of various genes in the intestine of both DSS-administered CHOP-null mice and WT mice. Tested genes included those for pro-inflammatory cytokines (*Il-1β*, *Tnf-α*, and *Il-6*), CAMs expressed on vascular endothelial cells (*Madcam-1*, *Vcam-1*, and *Icam-1*), CAMs expressed on leukocytes (*CD11b*, *CD49d*, and *L-selectin*), an anti-inflammatory cytokine (*Il-10*), and CHOP-regulated genes (*Caspase-11*, *Ero-1α*, and *Bcl-2*). Mac-1 and very late gene (VLA)-4 are CAMs expressed on leukocytes and Mac-1 is a heterodimer of CD11b and CD18 and VLA-4 is a heterodimer of CD49d and CD29. The mRNA expression of all of the pro-inflammatory cytokine genes tested was up-regulated by DSS administration, whereas the mRNA expression of *Tnf-α* but not that of *Il-1β* and *Il-6* was significantly lower in DSS-administered CHOP-null mice than in WT mice (Figure 4A). On the other hand, the mRNA expression of *Il-10* was higher in DSS-administered CHOP-null mice than in WT mice (Figure 4D).

The mRNA expression of all CAM genes tested was also up-regulated by DSS administration and the mRNA expression of *Vcam-1* and *CD11b* but not other CAM genes was significantly lower in DSS-administered CHOP-null mice than in WT mice (Figure 4, B and C). The mRNA expression of *Caspase-11* and *Ero-1α* but not *Bcl-2* was up-regulated by DSS administration in the WT mice, and the mRNA expression of *Caspase-11* and *Ero-1α* was significantly lower in DSS-administered CHOP-null mice than in WT mice (Figure 4, E and F).

The results in Figure 4 suggest that CHOP regulates the mRNA expression of *Tnf-α*, *Il-10*, *CD11b*, *Caspase-11*, and *Ero-1α* under inflammatory conditions. To test this idea *in vitro*, we compared the mRNA expression of these factors in the presence of LPS in peritoneal macrophages prepared from CHOP-null mice and WT mice. As shown in Figure 5A, LPS treatment stimulated the expression of *Chop* and *Grp78* mRNAs in macrophages in a CHOP-dependent manner. The mRNA expression of *CD11b*, *Caspase-11*, and *Ero-1α* was up-regulated by the LPS treatment, and the expression of these genes was significantly lower in LPS-treated CHOP-null macrophages

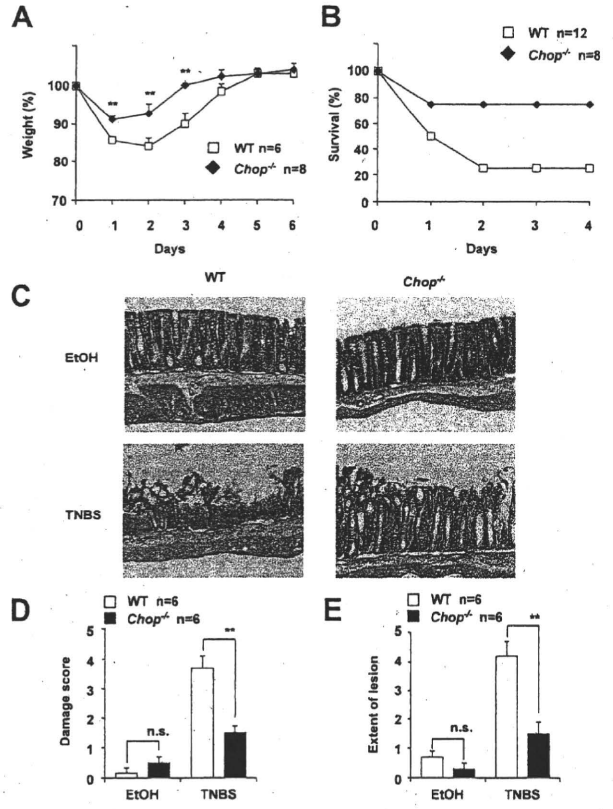

Figure 3. Development of TNBS-induced colitis in CHOP-null mice and WT mice. CHOP-null mice (*Chop*$^{-/-}$) and WT mice were intrarectally administered with (TNBS) or without (EtOH) TNBS of 3 mg/mouse (**A**, **C–E**) or 8 mg/mouse (**B**) once and cultivated for the indicated days. Body weight (**A**) and mouse survival rate (**B**) were measured daily. After 1 day, sections of colonic tissues were prepared and subjected to histological examination (H&E staining) as described in the legend of Figure 1, C–E. Values are mean ± SEM (n = 6 to 12). $^{**}P < 0.01$; n.s., not significant.

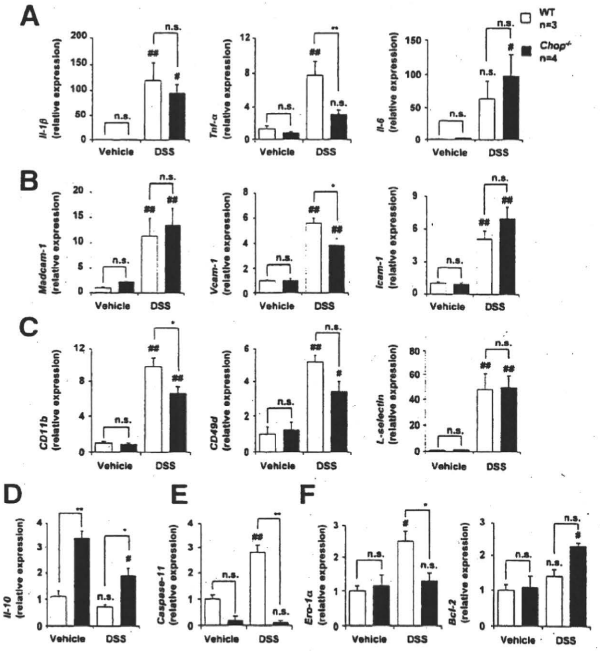

Figure 4. The mRNA expression of various genes in colonic tissues. DSS was administered to CHOP-null mice (*Chop*$^{-/-}$) and WT mice, as described in the legend of Figure 1. Relative mRNA expression of each gene in colonic tissues was monitored and expressed as described in the legend of Figure 2A. **A:** *IL-1β*, *TNF-α*, *IL-6*. **B:** *Madcam-1*, *Vcam-1*, *Icam-1*. **C:** *CD11b*, *CD49d*, *L-selectin*. **D:** *IL-10*. **E:** *Capsase-11*. **F:** *Ero-1α*, *Bcl-2*. Values are mean ± SEM (n = 4 to 5). ** or $^{\#\#}P < 0.01$; * or $^{\#}P < 0.05$; n.s., not significant.

than in the WT macrophages (Figure 5, C, E, and F). The mRNA expression of *Il-10* in the presence of LPS was higher in CHOP-null macrophages than in WT macrophages. However, no significant difference was found in the mRNA expression of *Tnf-α* (Figure 5, B and D). These results suggest that CHOP is involved in the expression of *CD11b*, *Caspase-11*, *Il-10*, and *Ero-1α* under inflammatory conditions, and that these may play an important role in CHOP-dependent exacerbation of DSS-induced colitis.

Involvement of IL-1β and Infiltration of Macrophages in the CHOP-Dependent Exacerbation of DSS-Induced Colitis

CHOP-induced expression of Caspase-11 and the resulting activation of Caspase-1 and stimulation of production of IL-1β are responsible for CHOP-dependent exacerbation of LPS-induced lung inflammation.[39] To test whether a similar mechanism is involved in the CHOP-dependent exacerbation of DSS-induced colitis, we measured the levels of IL-1β and Caspase-1 activity in colonic tissues in DSS-administered mice. As shown in Figure 6, A and B, DSS administration increased the level of IL-1β and

Caspase-1 activity in colonic tissues in WT mice. These alterations were significantly suppressed in CHOP-null mice. Similar results were observed in LPS-treated macrophages; the levels of IL-1β and the Caspase-1 activity

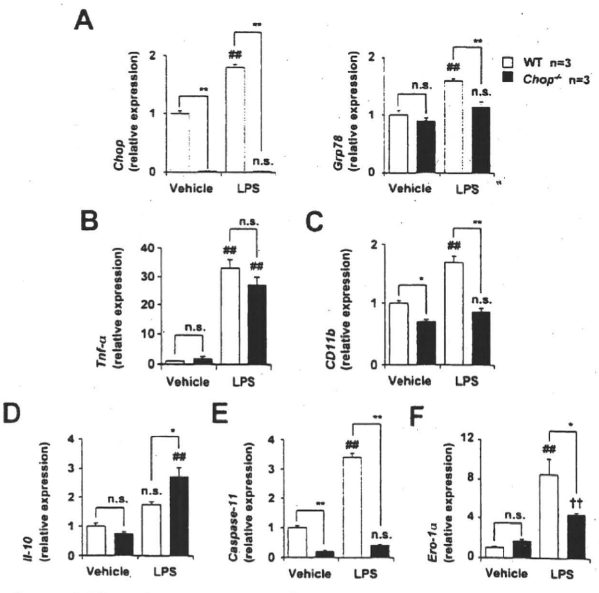

Figure 5. The mRNA expression of various genes in peritoneal macrophages. Peritoneal macrophages were prepared from CHOP-null mice (*Chop*$^{-/-}$) and WT mice and incubated with 10 ng/ml of LPS for 12 hours (3 hours for the *Tnf-α*). Relative mRNA expression of each gene in colonic tissues was monitored and expressed as described in the legend of Figure 2A. **A:** *Chop*, *Grp78*. **B:** *Tnf-α*. **C:** *CD11b*, **D:** *IL-10*. **E:** *Caspase-11*. **F:** *Ero-1α*. Values are mean ± SEM (n = 3). ** or $^{\#\#}P < 0.01$; * or $^{\#}P < 0.05$; n.s., not significant.

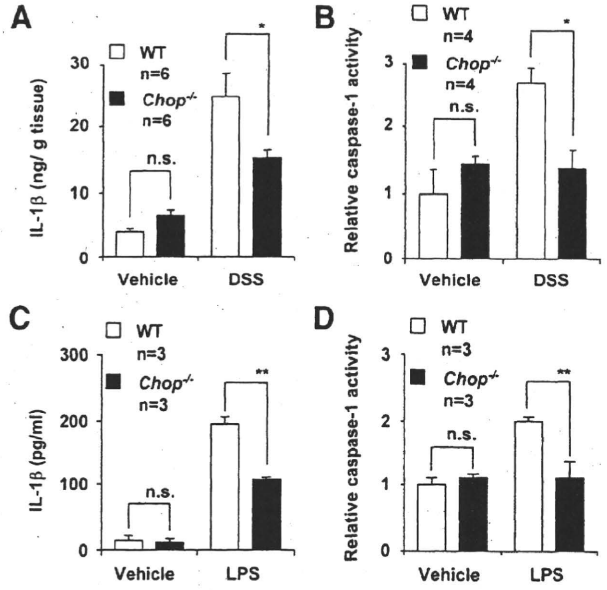

Figure 6. Involvement of Caspase-11-Caspase-1-IL-1β pathway in CHOP-dependent exacerbation of DSS-induced colitis. DSS was administered to CHOP-null mice (*Chop*$^{-/-}$) and wild-type mice (WT), as described in the legend of Figure 1, **A** and **B**. **C** and **D:** Peritoneal macrophages were prepared from CHOP-null mice (*Chop*$^{-/-}$) and WT mice and incubated with 10 ng/ml of LPS for 24 hours. **A** and **C:** The amount of IL-1β was determined by enzyme-linked immunosorbent assay. **B** and **D:** The Caspase-1 activity was measured as described in Materials and Methods. Values are mean ± SEM (n = 3 to 4). $^{**}P < 0.01$; $^{*}P < 0.05$; n.s., not significant.

in LPS-stimulated peritoneal macrophages prepared from CHOP-null mice were lower than in those from the WT mice (Figure 6, C and D).

Mac-1 is a CAM expressed on macrophages; its binding to ICAM-1 expressed on vascular endothelial cells is important for infiltration of blood-circulating macrophages into inflamed tissues.[43] To test whether infiltration of macrophages is involved in the CHOP-dependent exacerbation of DSS-induced colitis, we compared infiltration of macrophages between DSS-administered CHOP-null mice and the WT mice by immunohistochemical analysis with an antibody against CD68, which is expressed on lysosomal membranes of macrophages.[44] As shown in Figure 7A (see magnified panels), the antibody targeted mononuclear cells, confirming that this antibody can be used to detect macrophages. Results in Figure 7A show that DSS-induced infiltration of macrophages into colonic tissues was suppressed in CHOP-null mice compared with the WT mice. To confirm a role for CHOP in the expression of *CD11b* (Mac-1) *in vitro*, we used RAW264 cells (mouse leukemic monocyte) and plasmids for overexpression of CHOP and C/EBP-β, known to act coordinately with CHOP in the transcription of some genes.[45] As shown in Figure 7B, *CD11b* mRNA expression was up-regulated by transfection of cells with the plasmid with *Chop*, and this up-regulation was further stimulated by simultaneous transfection with a plasmid with *C/ebp-β*. We confirmed the overexpression of *Chop* and *C/ebp-β*, depending on the transfection of each plasmid (Figure 7, C and D). We found the CHOP-binding consensus sequences in the promoter of *CD11b* (Figure 7E). Overexpression of *C/ebp-β* did not affect the mRNA

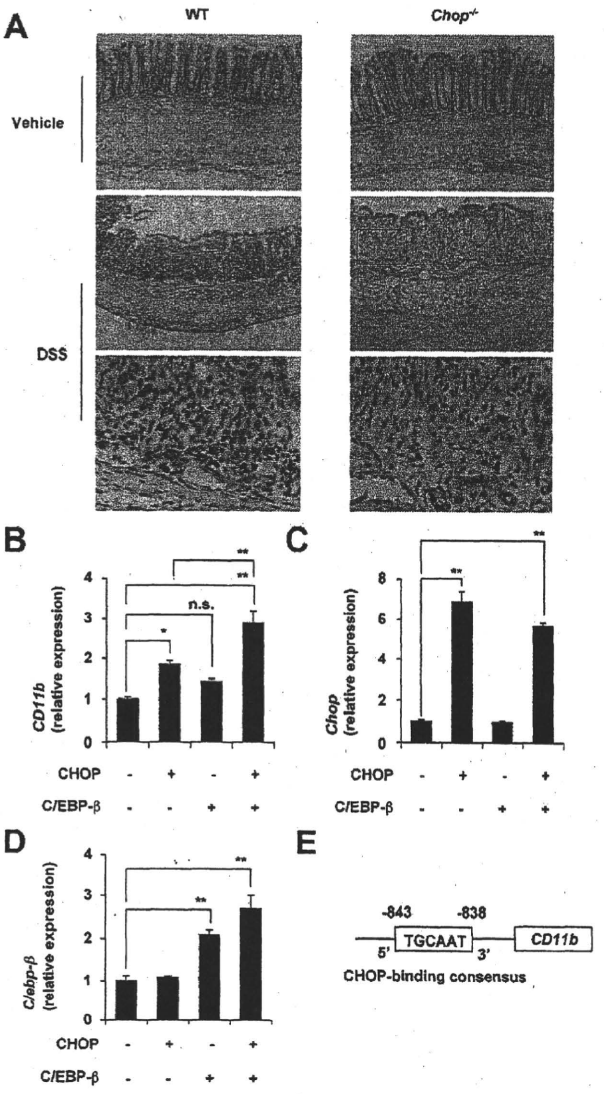

Figure 7. Involvement of infiltration of macrophages in CHOP-dependent exacerbation of DSS-induced colitis. DSS was administered to CHOP-null mice (*Chop*$^{-/-}$) and WT mice, as described in the legend of Figure 1. **A:** Sections of colonic tissues were prepared and subjected to immunohistochemical analysis with an antibody against CD68. The **bottom panel** in each column is a ×4 magnified image of the boxed area defined in the **middle panel**. RAW264 cells were transiently transfected with expression plasmid for CHOP and C/EBP-β and cultured for 12 hours. The relative mRNA expression of each gene was monitored and expressed as described in the legend of Figure 2A. **B–D:** Values are mean ± SEM (n = 3). $^{**}P < 0.01$; $^{*}P < 0.05$; n.s. not significant. **E:** The structure and sequences of the *CD11b* promoter are shown.

expression of *Chop*. Results in Figure 7 suggest that up-regulation of the expression of *CD11b* (Mac-1) by CHOP is involved in CHOP-dependent exacerbation of DSS-induced colitis through stimulation of macrophage infiltration into the intestine.

Involvement of ROS Production and ROS-Induced Apoptosis in Exacerbation of DSS-Induced Colitis

We measured ROS production in the intestine by measuring the lipid-derived free radical spin adduct with ESR

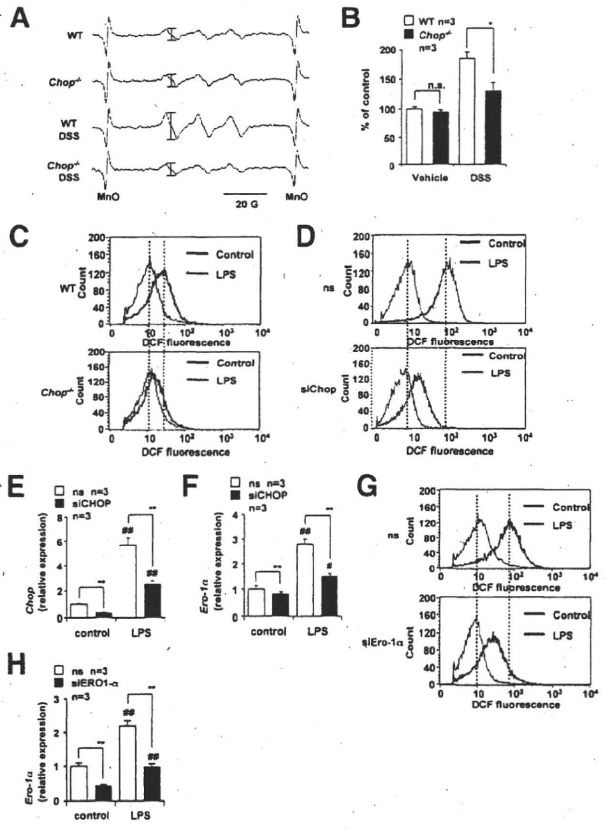

Figure 8. Involvement of ROS production in CHOP-dependent exacerbation of DSS-induced colitis. DSS was administered to CHOP-null mice (*Chop*$^{-/-}$) and wild-type mice (WT), as described in the legend of Figure 1. **A:** After administration of POBN, the colons were dissected and subjected to radical adduct ESR spectrum analysis. The intensity of the ESR signal of radical adduct (shown by bars) was determined, expressed relative to the control sample (ie, wild-type mice without DSS treatment), and given as the mean ± SEM (n = 3). **B:** $^{*}P < 0.05$; n.s., not significant. **C:** Peritoneal macrophages were prepared from CHOP-null mice (*Chop*$^{-/-}$) and WT mice and incubated with 10 ng/ml of LPS for 24 hours. **D–H:** RAW264 cells were transiently transfected with siRNA for CHOP (**D–F**) or ERO-1α (**G**, **H**) or nonsilencing (ns) siRNA (**D–H**) and incubated with 50 ng/ml of LPS for 24 hours. The production of ROS was monitored by fluorescence-activated cell sorting analysis with H_2DCF, as described in the Materials and Methods (**C**, **D**, and **G**). Relative mRNA expression of the *CHOP* (**E**) or *Ero-1α* (**F**, **H**) was monitored and expressed as described in the legend of Figure 2A. Values are mean ± SEM (n = 3). ** or $^{\#\#}P < 0.01$.

spectroscopy and spin trap POBN, which reacts with ROS to form a radical spin adduct. This method, *in vivo* free radical production *ex vivo* detection, was shown to be effective for monitoring ROS production in the lung *in vivo*.[41,42] However, this is the first attempt to use this technique on intestinal tissue. As shown in Figure 8A, a radical spin adduct of ESR spectrum similar to that reported in the lung was obtained. The hyperfine coupling constants for the POBN radical adducts were α^{N} = 14.91 ± 0.08 G and α^{H}_{β} = 2.45 ± 0.04 G, which are similar to data previously reported in the lung,[41,42] suggesting that this ESR spectrum is derived from lipid-derived free radicals and that this method can be used for the monitoring the ROS production at the intestine *in vivo*. As shown in Figure 8B, the level of ROS production in the intestine was elevated by DSS administration in the WT mice and lower in DSS-administered CHOP-null mice than in the WT mice. We also found that administration of vitamin E, an antioxidant, decreased the intestinal level of ROS production and the DAI in DSS-treated WT mice (Supplemental Figure 1 at *http://ajp.amjpathol.org*). Results suggest that the DSS-induced production of ROS in the intestine was suppressed in CHOP-null mice.

Production of ROS in peritoneal macrophages prepared from CHOP-null mice and WT mice was compared using fluorescence-activated cell sorting analysis. The cell-permeable fluorescent dye, H_2DCF, can be converted to a fluorescent product, DCF, in a ROS-dependent manner. Therefore, the increase in the green fluorescence (x axis in Figure 8, C, D, and G) is indicative of an increase in the level of ROS production.[40] Treatment of WT macrophages with LPS stimulated ROS production (Figure 8C), as has been described previously.[46] However, this stimulation was not clearly observed in CHOP-null macrophages, indicating that CHOP is responsible for LPS-stimulated ROS production (Figure 8C). We also examined the effect of siRNA for CHOP on LPS-stimulated ROS production in RAW264 cells (Figure 8D). We confirmed that treatment of RAW264 cells with LPS up-regulated the expression of *CHOP* mRNA and that transfection of cells with siRNA for CHOP significantly suppressed the expression of not only *CHOP* but also *Ero-1α* mRNA (Figure 8, E and F). As is the case with peritoneal macrophages, treatment of RAW264 cells with LPS stimulated ROS production and transfection of cells with siRNA for *CHOP* partially suppressed this LPS-stimulated ROS production (Figure 8D). To examine the role of ERO-1α in this CHOP-dependent production of ROS, we also examined the effect of siRNA for ERO-1α on LPS-stimulated ROS production in RAW264 cells. We confirmed that transfection of cells with siRNA for ERO-1α significantly suppressed the expression of *Ero-1α* mRNA (Figure 8H). Transfection of cells with siRNA for ERO-1α partially suppressed this LPS-stimulated ROS production (Figure 8G). Results in Figure 8 suggest that CHOP stimulates ROS production in macrophages at least partly through the up-regulation of ERO-1α.

Next, we compared the level of apoptosis in the colonic mucosa of DSS-administered CHOP-null mice and WT mice by use of the TUNEL assay. More TUNEL-positive cells (apoptosis) were observed in the colonic mucosa of DSS-administered WT mice than in CHOP-null mice (Figure 9A), suggesting that ROS-induced apoptosis associated with DSS-induced colitis is suppressed in CHOP-null mice.

To test the role of CHOP in ROS-induced apoptosis *in vitro*, we examined the effect of siRNA for CHOP on cell death induced by menadione, a superoxide anion (a representative ROS) releasing drug, in a colonic cancer cell line (HCT-15). We confirmed that transfection of cells with siRNA for CHOP inhibited the mRNA expression of *CHOP* in both the presence and absence of menadione (Figure 9B). As shown in Figure 9C, treatment of cells with menadione induced cell death in a dose-dependent manner, whereas transfection of cells with siRNA for CHOP significantly suppressed this menadione-induced cell death. We confirmed that cell death such as that evident in Figure 9C was mediated by apoptosis by showing that apoptotic DNA fragmentation and chroma-

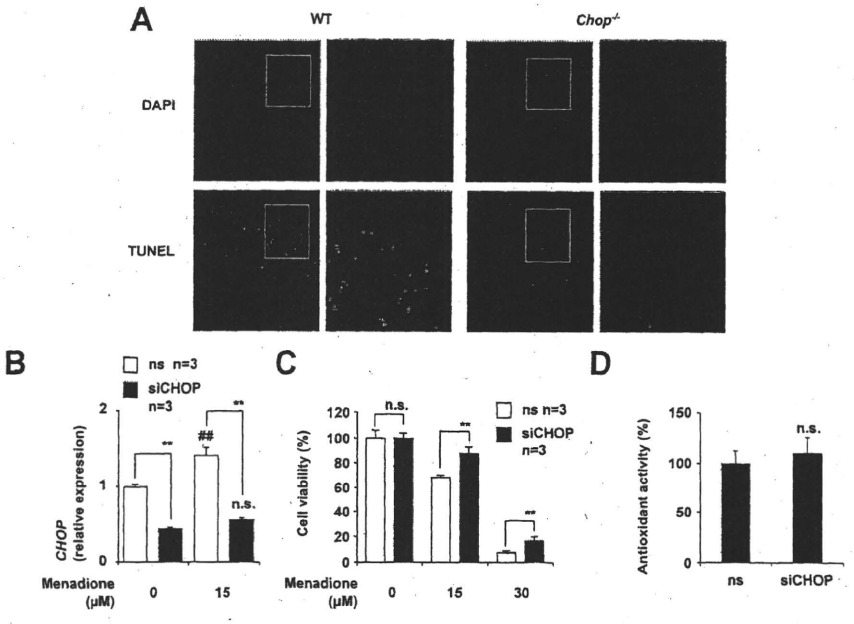

Figure 9. Involvement of ROS-induced apoptosis in CHOP-dependent exacerbation of DSS-induced colitis. DSS was administered to CHOP-null mice (*Chop*$^{-/-}$) and WT mice, as described in the legend of Figure 1. Sections of colonic tissues were prepared and subjected to TUNEL assay and DAPI staining. **A:** The **right panel** in each column is a ×3 magnified image of the boxed area defined in the **left panel**. HCT-15 cells were transfected with siRNA for CHOP (siCHOP) or nonsilencing (ns) siRNA and were incubated with indicated concentrations of menadione for 12 hours. **B:** Relative mRNA expression of the *CHOP* was monitored as described in the legend of Figure 2A. **C:** Cell viability was determined using the MTT method. **D:** The intracellular antioxidant activity was measured as described in the Materials and Methods. Values shown are mean ± SEM (n = 3). ** or **$P < 0.01$; n.s., not significant.

tin condensation accompanied the cell death (data not shown). The results in Figure 9 suggest that CHOP makes colonic cells sensitive to ROS-induced apoptosis, maybe through modulation of apoptosis-inducing pathway such as down-regulation of Bcl-2 and up-regulation of Bim.[16–18] We also examined the effect of CHOP on intracellular antioxidant activity. As shown in Figure 9D, the level of antioxidant activity that was measured by extinction of hydrogen peroxide was not affected by transfection of siRNA for CHOP. Results in Figures 8 and 9 imply that CHOP stimulates ROS-induced apoptosis through both increasing the ROS production and modulating the apoptosis-inducing pathway.

Discussion

CHOP is a transcription factor involved in the ER stress response, which has been recently revealed to play an important role in various diseases, including neurodegenerative diseases, diabetes, gastric ulcer, and lung inflammation.[24,39,47–50] However, its role in IBD has remained unknown. In this study, we obtained direct genetic evidence that CHOP stimulates the development of DSS- and TNBS-induced colitis, animal models of IBD, by showing that CHOP is up-regulated by DSS or TNBS administration and that CHOP-null mice are resistant to development of experimental colitis in these models. It was recently reported that IRE1β knockout mice are sensitive to DSS-induced colitis[51] and that up-regulation of GRP78 in IL-10 knockout mice contributes to spontaneous development of colitis through activation of nuclear factor-κB.[21] Thus, it seems that some aspects of the ER stress response are positively involved, and other aspects negatively involved, in the development of experimental colitis.

Our *in vivo* and *in vitro* analyses suggested that CHOP stimulates the development of DSS-induced colitis via several mechanisms. One of these is the Caspase-11-Casapse-1-IL-1β pathway, which was recently shown to play an important role in LPS-induced lung inflammation.[39] It is well-known that IL-1β stimulates the development of IBD and experimental colitis,[9] that CHOP positively regulates the transcription of *Caspase-11*, and that Caspase-11 activates Caspase-1, and that the production of IL-1β from pro-IL-1β is catalyzed by Caspase-1.[39] In this study, our *in vivo* analysis showed that the intestinal level of IL-1β and the activity of Caspase-1 was lower in DSS-administered CHOP-null mice than in WT mice. Because the production of IL-1β is stimulated under inflammatory conditions, it is possible that this decreased level of IL-1β is not a cause but a result of the amelioration of colitis in CHOP-null mice. However, we showed that up-regulation of *Caspase-11* mRNA expression and the activity of Caspase-1 in the intestine after DSS administration was suppressed in CHOP-null mice and in macrophages prepared from CHOP-null mice, compared with the respective WT control. These results suggest that the Caspase-11-Casapse-1-IL-1β pathway is involved in the CHOP-dependent exacerbation of DSS-induced colitis.

We also postulated that CHOP positively regulates the expression of *CD11b* (*Mac-1*) and that this mechanism is involved in CHOP-dependent exacerbation of DSS-induced colitis thorough stimulation of macrophage infiltration into the intestine. Mac-1 is expressed on the macrophage cell surface and stimulates the infiltration of blood-circulating macrophages into inflamed tissues.[43] In this study, we showed that *CD11b* (*Mac-1*) mRNA expression and infiltration of macrophages into the intestine were both reduced in DSS-administered CHOP-null mice compared with WT mice. We also showed that up-regulation or down-regulation of expression of *Chop* stimulates or suppresses, respectively, the expression of *CD11b* (*Mac-1*). Furthermore, we found the consensus DNA sequence for

CHOP binding in the promoter region of *CD11b*. Because IL-1β was reported to stimulate infiltration of macrophages,[52] lower levels of IL-1β in DSS-administered CHOP-null mice may contribute to their lower levels of macrophage infiltration. However, it is also possible that the CHOP-dependent inductions of *CD11b* (*Mac-1*) expression is attributable to the increased recruitment of Mac-1-positive myeloid cells.

We showed that intestinal ROS production is lower in DSS-administered CHOP-null mice than in WT mice and propose that this is one of the mechanisms governing the CHOP-dependent exacerbation of DSS-induced colitis. Although a number of *in vitro* studies have suggested that CHOP is involved in ROS production,[40,53] this is the first evidence showing that CHOP is involved in ROS production *in vivo*. We revealed this by use of radical spin adduct ESR spectrum analysis. This analysis should be useful for detecting intestinal ROS production *in vivo*. Furthermore, we suggested that the lower levels of ROS production in CHOP-null mice are attributable to the lower level of expression of ERO-1α; *Ero-1α* mRNA expression in the intestine in DSS-administered CHOP-null mice and ROS production in LPS-stimulated macrophages prepared from the mice were lower than in the respective WT control samples. Furthermore, we showed that siRNA for ERO-1α suppresses LPS-stimulated ROS production in RAW264 cells.

Analysis using the TUNEL assay revealed that DSS-induced apoptosis in colonic mucosa was inhibited in CHOP-null mice. This correlates with other parameters for DSS-induced colitis. However, it was not clear whether the alteration to apoptosis is caused by or is a result of the inhibition of DSS-induced colitis. Given that transfection with siRNA for CHOP inhibited ROS-induced apoptosis *in vitro*, this result suggests that CHOP stimulates ROS-induced apoptosis, which seems to contribute to the lower level of apoptosis in the colonic mucosa and to a phenotype resistant to DSS-induced colitis as seen in CHOP-null mice. A number of mechanisms have been proposed for the stimulation of apoptosis by CHOP, such as down-regulation of Bcl-2, translocation of BAX to mitochondria, and activation of Bim.[16,40,54] Because we showed that *Bcl-2* mRNA expression was not affected by the lack of *Chop*, other mechanisms seem to be involved. It is also possible that activation of Caspase-11 is involved in the stimulation of ROS-induced apoptosis by CHOP, because Caspase-11 stimulates the activation of capsase-3 and Caspase-7, both of which are directly involved in the induction of apoptosis.[55]

In addition to the mechanisms described above, other mechanisms may be involved in the CHOP-dependent exacerbation of DSS-induced colitis, such as down-regulation of IL-10 and up-regulation of GRP78. IL-10 was reported to suppress development of IBD and experimental colitis,[56] whereas expression of GRP78 stimulates the development of DSS-induced colitis through activation of nuclear factor-κB.[21] We showed here that expression of *Il-10* or *Grp78* mRNA in the intestine of DSS-administered CHOP-null mice was higher or lower, respectively, than in the WT control.

Glucocorticoids, 5-aminosalicylic acid (5-ASA), and immunosuppressive drugs are currently used for the clinical treatment of IBD.[2] Although some new types of drugs, such as infliximab, have been developed recently for the treatment of IBD, a number of clinical problems, such as side effects, are yet to be addressed.[57] Thus, IBD remains an uncured disease for which the development of new types of drugs is clinically important. As described above, some aspects of the ER stress response are positively and other aspects negatively involved in IBD development. As such, factors located downstream (such as CHOP) rather than upstream (such as ATF6 and IRE1) of the ER stress response may be better drug targets for IBD. Results in this study suggest that inhibitors of CHOP may be therapeutically beneficial for IBD.

In summary, results in this study show that CHOP is positively involved in the development of DSS-induced colitis. Furthermore, the results suggest that this effect involves various mechanisms, such as Mac-1-induced infiltration of macrophages, ERO-1α-induced ROS production, Caspase-11-induced production of IL-1β, and stimulation of mucosal apoptosis.

Acknowledgment

We thank Dr. Akira Shizuo (Osaka University, Osaka, Japan) for generously providing the mice.

References

1. Cuzzocrea S: Emerging biotherapies for inflammatory bowel disease. Expert Opin Emerg Drugs 2003, 8:339–347
2. Podolsky DK: Inflammatory bowel disease. N Engl J Med 2002, 347:417–429
3. Jurjus AR, Khoury NN, Reimund JM: Animal models of inflammatory bowel disease. J Pharmacol Toxicol Methods 2004, 50:81–92
4. Danese S, Semeraro S, Marini M, Roberto I, Armuzzi A, Papa A, Gasbarrini A: Adhesion molecules in inflammatory bowel disease: therapeutic implications for gut inflammation. Dig Liver Dis 2005, 37:811–818
5. Reinecker HC, Steffen M, Witthoeft T, Pflueger I, Schreiber S, MacDermott RP, Raedler A: Enhanced secretion of tumour necrosis factor-alpha, IL-6, and IL-1 beta by isolated lamina propria mononuclear cells from patients with ulcerative colitis and Crohn's disease. Clin Exp Immunol 1993, 94:174–181
6. Elson CO, Sartor RB, Tennyson GS, Riddell RH: Experimental models of inflammatory bowel disease. Gastroenterology 1995, 109:1344–1367
7. Koizumi M, King N, Lobb R, Benjamin C, Podolsky DK: Expression of vascular adhesion molecules in inflammatory bowel disease. Gastroenterology 1992, 103:840–847
8. Kinoshita K, Hori M, Fujisawa M, Sato K, Ohama T, Momotani E, Ozaki H: Role of TNF-alpha in muscularis inflammation and motility disorder in a TNBS-induced colitis model: clues from TNF-alpha-deficient mice. Neurogastroenterol Motil 2006, 18:578–588
9. Maeda S, Hsu LC, Liu H, Bankston LA, Iimura M, Kagnoff MF, Eckmann L, Karin M: Nod2 mutation in Crohn's disease potentiates NF-kappaB activity and IL-1beta processing. Science 2005, 307:734–738
10. Palmen MJ, Dijkstra CD, van der Ende MB, Pena AS, van Rees EP: Anti-CD11b/CD18 antibodies reduce inflammation in acute colitis in rats. Clin Exp Immunol 1995, 101:351–356
11. Leon F, Contractor N, Fuss I, Marth T, Lahey E, Iwaki S, la Sala A, Hoffmann V, Strober W, Kelsall BL: Antibodies to complement

receptor 3 treat established inflammation in murine models of colitis and a novel model of psoriasiform dermatitis. J Immunol 2006, 177:6974–6982
12. Bendjelloul F, Maly P, Mandys V, Jirkovska M, Prokesova L, Tuckova L, Tlaskalova-Hogenova H: Intercellular adhesion molecule-1 (ICAM-1) deficiency protects mice against severe forms of experimentally induced colitis. Clin Exp Immunol 2000, 119:57–63
13. Yacyshyn BR, Bowen-Yacyshyn MB, Jewell L, Tami JA, Bennett CF, Kisner DL, Shanahan Jr WR: A placebo-controlled trial of ICAM-1 antisense oligonucleotide in the treatment of Crohn's disease. Gastroenterology 1998, 114:1133–1142
14. Targan SR, Hanauer SB, van Deventer SJ, Mayer L, Present DH, Braakman T, DeWoody KL, Schaible TF, Rutgeerts PJ: A short-term study of chimeric monoclonal antibody cA2 to tumor necrosis factor alpha for Crohn's disease. Crohn's Disease cA2 Study Group. N Engl J Med 1997, 337:1029–1036
15. Rutgeerts P, Van Assche G, Vermeire S: Optimizing anti-TNF treatment in inflammatory bowel disease. Gastroenterology 2004, 126:1593–1610
16. Puthalakath H, O'Reilly LA, Gunn P, Lee L, Kelly PN, Huntington ND, Hughes PD, Michalak EM, McKimm-Breschkin J, Motoyama N, Gotoh T, Akira S, Bouillet P, Strasser A: ER stress triggers apoptosis by activating BH3-only protein Bim. Cell 2007, 129:1337–1349
17. Oyadomari S, Mori M: Roles of CHOP/GADD153 in endoplasmic reticulum stress. Cell Death Differ 2004, 11:381–389
18. Zinszner H, Kuroda M, Wang X, Batchvarova N, Lightfoot RT, Remotti H, Stevens JL, Ron D: CHOP is implicated in programmed cell death in response to impaired function of the endoplasmic reticulum. Genes Dev 1998, 12:982–995
19. Xue X, Piao JH, Nakajima A, Sakon-Komazawa S, Kojima Y, Mori K, Yagita H, Okumura K, Harding H, Nakano H: Tumor necrosis factor alpha (TNFalpha) induces the unfolded protein response (UPR) in a reactive oxygen species (ROS)-dependent fashion, and the UPR counteracts ROS accumulation by TNFalpha. J Biol Chem 2005, 280:33917–33925
20. Zhang K, Shen X, Wu J, Sakaki K, Saunders T, Rutkowski DT, Back SH, Kaufman RJ: Endoplasmic reticulum stress activates cleavage of CREBH to induce a systemic inflammatory response. Cell 2006, 124:587–599
21. Shkoda A, Ruiz PA, Daniel H, Kim SC, Rogler G, Sartor RB, Haller D: Interleukin-10 blocked endoplasmic reticulum stress in intestinal epithelial cells: impact on chronic inflammation. Gastroenterology 2007, 132:190–207
22. Burczynski ME, Peterson RL, Twine NC, Zuberek KA, Brodeur BJ, Casciotti L, Maganti V, Reddy PS, Strahs A, Immermann F, Spinelli W, Schwertschlag U, Slager AM, Cotreau MM, Dorner AJ: Molecular classification of Crohn's disease and ulcerative colitis patients using transcriptional profiles in peripheral blood mononuclear cells. J Mol Diagn 2006, 8:51–61
23. Tanaka K, Namba T, Arai Y, Fujimoto M, Adachi H, Sobue G, Takeuchi K, Nakai A, Mizushima T: Genetic evidence for a protective role for heat shock factor 1 and heat shock protein 70 against colitis. J Biol Chem 2007, 282:23240–23252
24. Oyadomari S, Takeda K, Takiguchi M, Gotoh T, Matsumoto M, Wada I, Akira S, Araki E, Mori M: Nitric oxide-induced apoptosis in pancreatic beta cells is mediated by the endoplasmic reticulum stress pathway. Proc Natl Acad Sci USA 2001, 98:10845–10850
25. Rumi G, Tsubouchi R, Nishio H, Kato S, Mozsik G, Takeuchi K: Dual role of endogenous nitric oxide in development of dextran sodium sulfate-induced colitis in rats. J Physiol Pharmacol 2004, 55:823–836
26. Nishihara T, Matsuda M, Araki H, Oshima K, Kihara S, Funahashi T, Shimomura I: Effect of adiponectin on murine colitis induced by dextran sulfate sodium. Gastroenterology 2006, 131:853–861
27. Krawisz JE, Sharon P, Stenson WF: Quantitative assay for acute intestinal inflammation based on myeloperoxidase activity. Assessment of inflammation in rat and hamster models. Gastroenterology 1984, 87:1344–1350
28. Bradford MM: A rapid and sensitive method for the quantitation of microgram quantities of protein utilizing the principle of protein-dye binding. Anal Biochem 1976, 72:248–254
29. Rumi G, Tsubouchi R, Okayama M, Kato S, Mozsik G, Takeuchi K: Protective effect of lactulose on dextran sulfate sodium-induced colonic inflammation in rats. Dig Dis Sci 2004, 49:1466–1472
30. Ohkawa H, Ohishi N, Yagi K: Assay for lipid peroxides in animal tissues by thiobarbituric acid reaction. Anal Biochem 1979, 95:351–358
31. Tanaka K, Tsutsumi S, Arai Y, Hoshino T, Suzuki K, Takaki E, Ito T, Takeuchi K, Nakai A, Mizushima T: Genetic evidence for a protective role of heat shock factor 1 against irritant-induced gastric lesions. Mol Pharmacol 2007, 71:985–993
32. Tsutsumi S, Tomisato W, Takano T, Rokutan K, Tsuchiya T, Mizushima T: Gastric irritant-induced apoptosis in guinea pig gastric mucosal cells in primary culture. Biochim Biophys Acta 2002, 1589:168–180
33. Mima S, Tsutsumi S, Ushijima H, Takeda M, Fukuda I, Yokomizo K, Suzuki K, Sano K, Nakanishi T, Tomisato W, Tsuchiya T, Mizushima T: Induction of claudin-4 by nonsteroidal anti-inflammatory drugs and its contribution to their chemopreventive effect. Cancer Res 2005, 65:1868–1876
34. Ohkawara T, Nishihira J, Takeda H, Hige S, Kato M, Sugiyama T, Iwanaga T, Nakamura H, Mizue Y, Asaka M: Amelioration of dextran sulfate sodium-induced colitis by anti-macrophage migration inhibitory factor antibody in mice. Gastroenterology 2002, 123:256–270
35. Cooper HS, Murthy SN, Shah RS, Sedergran DJ: Clinicopathologic study of dextran sulfate sodium experimental murine colitis. Lab Invest 1993, 69:238–249
36. Nishiyori A, Tashiro H, Kimura A, Akagi K, Yamamura K, Mori M, Takiguchi M: Determination of tissue specificity of the enhancer by combinatorial operation of tissue-enriched transcription factors. Both HNF-4 and C/EBP beta are required for liver-specific activity of the ornithine transcarbamylase enhancer. J Biol Chem 1994, 269:1323–1331
37. Gotoh T, Oyadomari S, Mori K, Mori M: Nitric oxide-induced apoptosis in RAW 264.7 macrophages is mediated by endoplasmic reticulum stress pathway involving ATF6 and CHOP. J Biol Chem 2002, 277:12343–12350
38. Salimuddin, Nagasaki A, Gotoh T, Isobe H, Mori M: Regulation of the genes for arginase isoforms and related enzymes in mouse macrophages by lipopolysaccharide. Am J Physiol 1999, 277:E110–E117
39. Endo M, Mori M, Akira S, Gotoh T: C/EBP homologous protein (CHOP) is crucial for the induction of caspase-11 and the pathogenesis of lipopolysaccharide-induced inflammation. J Immunol 2006, 176:6245–6253
40. McCullough KD, Martindale JL, Klotz LO, Aw TY, Holbrook NJ: Gadd153 sensitizes cells to endoplasmic reticulum stress by down-regulating Bcl2 and perturbing the cellular redox state. Mol Cell Biol 2001, 21:1249–1259
41. Sato K, Kadiiska MB, Ghio AJ, Corbett J, Fann YC, Holland SM, Thurman RG, Mason RP: In vivo lipid-derived free radical formation by NADPH oxidase in acute lung injury induced by lipopolysaccharide: a model for ARDS. FASEB J 2002, 16:1713–1720
42. Sato K, Akaike T, Kohno M, Ando M, Maeda H: Hydroxyl radical production by H2O2 plus Cu,Zn-superoxide dismutase reflects the activity of free copper released from the oxidatively damaged enzyme. J Biol Chem 1992, 267:25371–25377
43. Diamond MS, Staunton DE, de Fougerolles AR, Stacker SA, Garcia-Aguilar J, Hibbs ML, Springer TA: ICAM-1 (CD54): a counter-receptor for Mac-1 (CD11b/CD18). J Cell Biol 1990, 111:3129–3139
44. Shah YM, Morimura K, Gonzalez FJ: Expression of peroxisome proliferator-activated receptor-gamma in macrophage suppresses experimentally induced colitis. Am J Physiol 2007, 292:G657–G666
45. Ohoka N, Yoshii S, Hattori T, Onozaki K, Hayashi H: TRB3, a novel ER stress-inducible gene, is induced via ATF4-CHOP pathway and is involved in cell death. EMBO J 2005, 24:1243–1255
46. Hsu HY, Wen MH: Lipopolysaccharide-mediated reactive oxygen species and signal transduction in the regulation of interleukin-1 gene expression. J Biol Chem 2002, 277:22131–22139
47. Oyadomari S, Araki E, Mori M: Endoplasmic reticulum stress-mediated apoptosis in pancreatic beta-cells. Apoptosis 2002, 7:335–345
48. Tsutsumi S, Gotoh T, Tomisato W, Mima S, Hoshino T, Hwang HJ, Takenaka H, Tsuchiya T, Mori M, Mizushima T: Endoplasmic reticulum stress response is involved in nonsteroidal anti-inflammatory drug-induced apoptosis. Cell Death Differ 2004, 11:1009–1016
49. Milhavet O, Martindale JL, Camandola S, Chan SL, Gary DS, Cheng A, Holbrook NJ, Mattson MP: Involvement of Gadd153 in the pathogenic action of presenilin-1 mutations. J Neurochem 2002, 83:673–681
50. Holtz WA, O'Malley KL: Parkinsonian mimetics induce aspects of

unfolded protein response in death of dopaminergic neurons. J Biol Chem 2003, 278:19367–19377
51. Bertolotti A, Wang X, Novoa I, Jungreis R, Schlessinger K, Cho JH, West AB, Ron D: Increased sensitivity to dextran sodium sulfate colitis in IRE1beta-deficient mice. J Clin Invest 2001, 107:585–593
52. Bry K, Whitsett JA, Lappalainen U: IL-1beta disrupts postnatal lung morphogenesis in the mouse. Am J Respir Cell Mol Biol 2007, 36:32–42
53. Bek MF, Bayer M, Muller B, Greiber S, Lang D, Schwab A, August C, Springer E, Rohrbach R, Huber TB, Benzing T, Pavenstadt H: Expression and function of C/EBP homology protein (GADD153) in podocytes. Am J Pathol 2006, 168:20–32
54. Gotoh T, Terada K, Oyadomari S, Mori M: hsp70-DnaJ chaperone pair prevents nitric oxide- and CHOP-induced apoptosis by inhibiting translocation of Bax to mitochondria. Cell Death Differ 2004, 11:390–402
55. Kang SJ, Wang S, Kuida K, Yuan J: Distinct downstream pathways of caspase-11 in regulating apoptosis and cytokine maturation during septic shock response. Cell Death Differ 2002, 9:1115–1125
56. Kühn R, Lohler J, Rennick D, Rajewsky K, Muller W: Interleukin-10-deficient mice develop chronic enterocolitis. Cell 1993, 75:263–274
57. Keane J, Gershon S, Wise RP, Mirabile-Levens E, Kasznica J, Schwieterman WD, Siegel JN, Braun MM: Tuberculosis associated with infliximab, a tumor necrosis factor alpha-neutralizing agent. N Engl J Med 2001, 345:1098–1104

Highlighted paper selected by Editor-in-chief

Effect of Claudin Expression on Paracellular Permeability, Migration and Invasion of Colonic Cancer Cells

Masaya TAKEHARA, Tomoko NISHIMURA, Shinji MIMA, Tatsuya HOSHINO, and Tohru MIZUSHIMA*

Graduate School of Medical and Pharmaceutical Sciences, Kumamoto University; Kumamoto 862–0973, Japan.
Received February 10, 2009; accepted February 12, 2009; published online February 18, 2009

Alteration in the expression of claudins, consisting of tight junctions (TJs), has been reported in various clinically isolated tumors. Claudins play an important role not only in the intercellular barrier function of TJs but also in migration and invasiveness of cancer cells. However, the use of different types of cells and different claudins in these studies has complicated the picture. In this study, we systematically examined the effect of claudin (claudin-1, -2, -3, -4 and -15) overexpression on the paracellular permeability, migration and invasiveness of Caco-2 colonic cancer cells. Overexpression of claudin-4 or claudin-2 increased or decreased, respectively, paracellular permeability. Overexpression of claudin-4 specifically stimulated the invasive activity of the Caco-2 cells. Furthermore, activation of matrix metalloproteinase (MMP)-2 and MMP-9 were observed in the claudin-4-overexpressing cells, suggesting that the invasive activity was stimulated through an increase in MMP activity. Overexpression of claudin-2 or claudin-3 and -4 stimulated or inhibited, respectively, the migration activity of the Caco-2 cells. Immunostaining analysis revealed that each of the overexpressed claudins localized at TJs under the conditions used to evaluate paracellular permeability. In contrast, they localized mainly in intracellular compartments under experimental conditions designed to assess cell invasion and migration. Overall, the results of this study show that the effect exerted by the claudins on the intercellular barrier function of TJs, as well as on cell migration and invasive activity, differs depending on the particular claudin species. Furthermore, the subcellular localization of the claudins varies according to the culture conditions.

Key words tight junction; claudin; invasion; permeability; cancer

Tight junctions (TJs), the most apical intercellular structures in epithelial and endothelial cells, create a physiological intercellular barrier separating the apical and basolateral spaces, as well as regulating the paracellular permeability of various solutes. They also act as a divide between the apical and basolateral membranes, thereby maintaining cell polarity. TJs contain transmembrane proteins such as claudins, occludin and junctional adhesion molecules. The C-terminal regions of these proteins interact with cytosolic proteins, such as zonula occludens (ZO)-1, -2 and -3, which are linked to the actin cytoskeleton and are potentially involved in signal transduction.[1—6] Among these transmembrane proteins, the claudin family of proteins (claudin-1 to -24) play a major role in maintaining the intercellular barrier.[7,8]

Given that a loss of TJ structure and function is frequently observed in epithelium-derived cancers,[9—12] TJs have attracted considerable attention in relation to this disease. The loss of TJ structure and function is thought to promote cancer cell proliferation by allowing constitutive accessibility of cancers to nutrients and growth factors. As TJs function as a barrier against cancer cell invasion, loss of TJ structure and function could also stimulate the metastasis of tumors.[11,13—15]

Alteration in the expression of the constituent proteins of TJs, in particular claudins, is frequently observed in tumors clinically isolated from various types of tissues, including colon, breast, pancreas, prostate, uterus and ovary.[9—12,16—20] It was initially believed that these alterations in expression affect cancer development only through the modulation of the barrier function of TJs. However, a number of recent studies suggest that the expression of certain claudins modulates the invasiveness and migration of cancer cells through various mechanisms.[9,11] For example, we recently reported that overexpression of claudin-4 or claudin-2 causes a decrease or an increase, respectively, in the migration activity of gastric carcinoma (AGS) cells.[21,22] Studies from other groups have also shown that claudin overexpression (claudin-1, 3, 4, 5) can affect the invasiveness and migration of various types of cancer cells.[16,23—26]

Thus, an alteration in claudin expression appears to play a role in the progression of tumors, both by modulating the barrier function of TJs and by altering the migration and invasiveness of the cancer cells. However, the overall relationship between claudin expression and these cell functions have not been fully elucidated, partly due to the different types of cells and different cell culture conditions (*i.e.* cell density) used in the various studies. For example, although we showed that overexpression of claudin-4 decreases cell migration activity in AGS cells, other groups have reported that the overexpression stimulates cell invasion and migration in human ovarian cancer cells,[25] but inhibits the invasiveness of pancreatic cancer cells.[16] The relationship between the barrier function of TJs and cell migration and invasion also remains unclear, as these two functions were not investigated simultaneously in most studies. Furthermore, the subcellular localization of overexpressed claudins is still open to debate; some reports have demonstrated their localization at TJs whereas others have described their localization in intracellular component.[24,27—29] In this study, we selected Caco-2 cells (human carcinoma cell line derived from colon) for investigation of these issues, as functional TJs can be formed in these cells, and assay systems for their invasion and migration activities have been established.[30,31] Our results reveal that the TJ intercellular barrier function, as well as cell migration and invasion, are affected differently, depending on the claudin species being overexpressed. We also found that subcellular localization of claudins alters according to the culture conditions.

* To whom correspondence should be addressed. e-mail: mizu@gpo.kumamoto-u.ac.jp

MATERIALS AND METHODS

Chemicals and Media Dulbecco's modified Eagle's medium (DMEM) was obtained from Nissui Pharmaceutical Co. Fetal bovine serum (FBS), fibronectin and G418 were purchased from Sigma, non-essential amino acids (NEAAs) from BioWhittaker, and lipofectamine (TM2000) and pcDNA3.1(−) from Invitrogen. The RNeasy kit was obtained from Qiagen, the first-strand cDNA synthesis kit came from GE Healthcare and iQ SYBR Green Supermix was from Bio-Rad. Matrigel was purchased from BD Biosciences and the 24-well transwells were from Costar. Antibodies against claudin-1, claudin-2, claudin-3, claudin-15 and ZO-1 were from Zymed and those against claudin-4, occludin and actin were from Santa Cruz Biotechnology. Fluorescein isothiocyanate-dextran (4 kDa; FD4) was obtained from Fluka Biochemika.

Cell Culture and Plasmid Construction for Overexpression of Claudins Caco-2 cells were cultured in DMEM containing 10% FBS.

Full-length human *claudin-1*, *-3* and *-15* cDNAs were polymerase chain reaction (PCR)-amplified, using genome prepared from Caco-2 cells, and cloned into pcDNA3.1(−) to create the plasmid for overexpression of each claudin. The construction of the overexpression of plasmids for claudin-2 and claudin-4 was previously described.[21,22]

Transfection of Caco-2 cells with plasmids was carried out using Lipofectamine (TM2000) according to the manufacturer's protocols. The stable transfectants expressing each claudin were selected by immunoblotting analysis. Positive clones were maintained in the presence of 400 μg/ml G418.

Gelatin Zymography The proteolytic activity of matrix metalloproteinase (MMP)-2 and -9 was assessed by sodium dodecyl sulfate-polyacrylamide gel electrophoresis (SDS)-PAGE using zymogram gels containing 0.1% (w/v) gelatin, as described previously.[32] The culture medium was concentrated and the protein concentration was determined according to the Bradford method.[33] Following electrophoresis at 4 °C, the gels were washed with 2.5% Triton X-100 for 1 h at 37 °C and incubated with zymogram development buffer for 2 d at 37 °C. Bands were visualized by staining with Coomassie Brilliant Blue.

Real-Time Reverse Transcription (RT)-PCR Total RNA was extracted using an RNeasy kit according to the manufacturer's protocol. Samples (2.5 μg RNA) were reverse-transcribed using a first-strand cDNA synthesis kit according to the manufacturer's instructions. Synthesized cDNA was used in real-time RT-PCR (Chromo 4 instrument; Bio-Rad) experiments using iQ SYBR GREEN Supermix, and analyzed with Opticon Monitor Software according to the manufacturer's instructions. The real-time PCR cycle conditions were 2 min at 50 °C, followed by 10 min at 90 °C and finally 45 cycles of 95 °C for 30 s and 63 °C for 60 s. Specificity was confirmed by electrophoretic analysis of the reaction products and by inclusion of template- or reverse transcriptase-free controls. To normalize the amount of total RNA present in each reaction, *actin* cDNA was used as an internal standard.

Immunoblotting Analysis Whole cell extracts were prepared as described previously.[21] The protein concentration of the sample was determined by the Bradford method.[33] Samples were applied to 12% polyacrylamide gels containing SDS, subjected to electrophoresis, and proteins then immunoblotted with each antibody.

Cell Invasion Assay The cell invasion activity was measured by transwell matrigel invasion assay as described previously,[34] with some modifications. Serum-free medium containing 5 mg/ml matrigel was applied to the upper chamber of a 24-well transwell and incubated at 37 °C for 4 h. The cell suspension was applied to the matrigel and the lower chamber was filled with medium containing 10% FBS and 5 μg/ml fibronectin. The plate was incubated at 37 °C for 48 h. Cells were removed from the upper surface of the membrane and the lower surface of the membrane was stained for 10 min with 0.5% crystal violet in 25% methanol, rinsed with distilled water and air-dried overnight. The crystal violet was then extracted with 0.1 M sodium citrate in 50% ethanol and the absorbance was measured at 585 nm.

Cell Migration Assay Cells in serum-free medium were applied to the upper chamber of the transwell and the lower chamber was filled with medium containing 10% FBS and 5 μg/ml fibronectin. The plate was incubated at 37 °C for 48 h, and migrated cell were assessed as described for cell invasion assay.

Immunofluorescence Microscopy Caco-2 cells were grown in the Lab-Tek II chamber slide system (Nalge Nunc International). Cells were fixed in ice-cold methanol or acetone for 20 min and blocked in phosphate buffered saline (PBS) containing 3% bovine serum albumin (BSA) for 30 min. The samples were then incubated with each primary antibody. After washing, samples were incubated with the respective secondary antibody conjugated with Alexa Fluor 594 or Alexa Fluor 488 (Molecular Probes). Images were captured on a confocal laser-scanning fluorescence microscope (FLUOVIEW FV500-IX-UV, Olympus).

Measurement of Transepithelial Resistance (TER) Caco-2 cells were seeded at an initial density of 4.3×10^5 cells/cm^2 in the upper chamber of transwells. The cells were incubated at 37 °C for 7 d, with a change of medium every second day. TER was measured using an epithelial voltohmmeter (Millipore). The results were expressed as the measured resistance in Ohms multiplied by the area of the filter (0.33 cm^2).

Permeability Assay for Fluorescein Isothiocyanate (FITC)-Dextran We determined the permeability of Caco-2 cells by measuring transepithelial passage of FD4. The cells were seeded in the upper chamber of a 24-well transwell and incubated at 37 °C for 7 d. FD4 (5 mg/ml) was added to the upper chamber. Aliquots were withdrawn from the lower chambers after 4 h and measured for fluorescence at 520 nm with excitation at 485 nm. An apparent permeability coefficient (P_{app}) was calculated as described previously.[35]

Statistical Analysis All values are expressed as the mean±standard deviation (S.D.). Two-way analysis of variance (ANOVA), followed by the Tukey test or the Student's *t*-test for unpaired results, was used to evaluate differences between more than three groups or between two groups, respectively. Differences were considered to be significant for values of $p<0.05$.

RESULTS

Overexpression of Claudins and Their Subcellualr Lo-

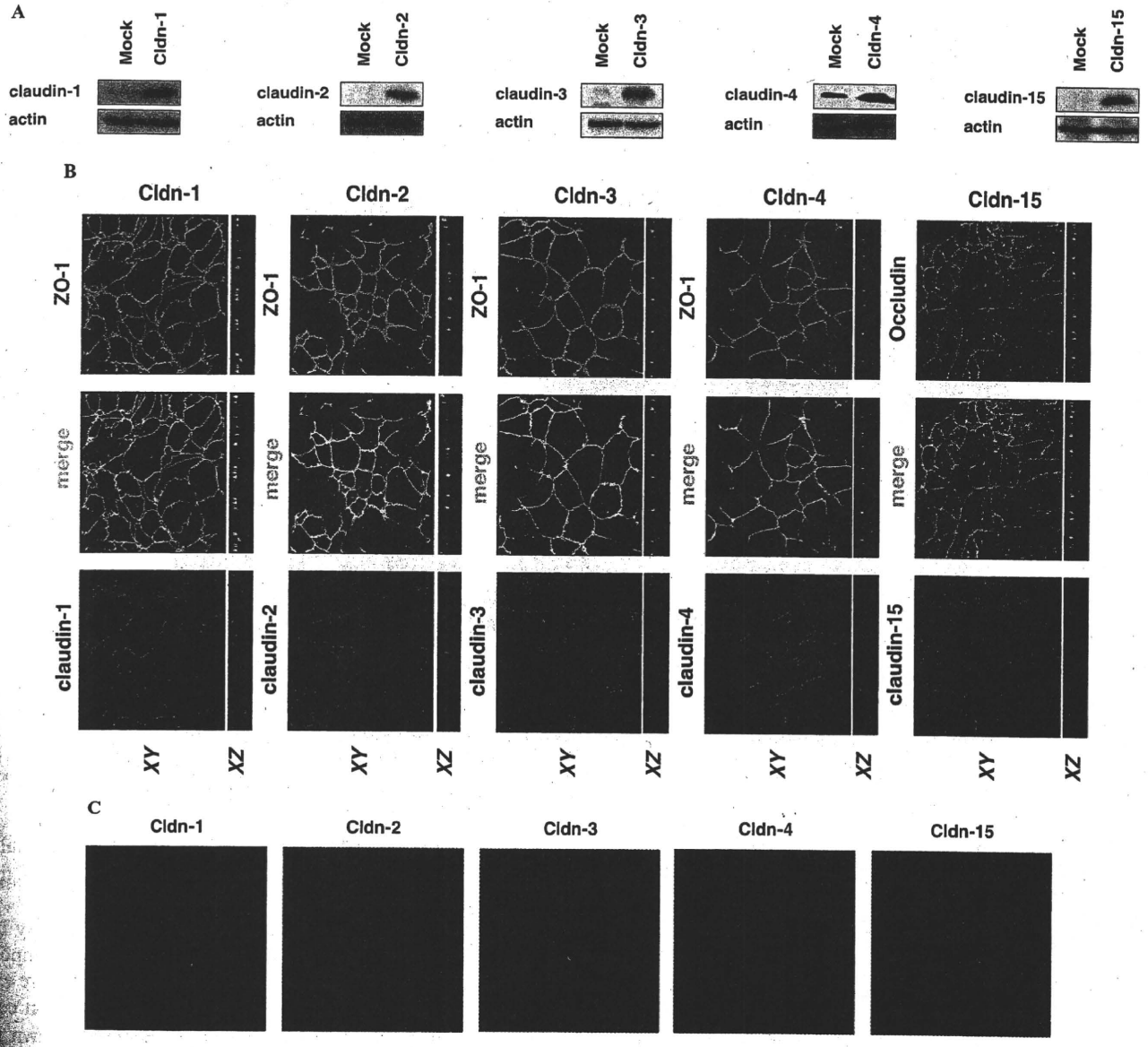

Fig. 1. Overexpression of Claudins and Their Localization in Caco-2 Cells

Caco-2 cells stably transfected with claudin-1, -2, -3, -4 or -15 expression plasmid (Cldn-1, -2, -3, -4 or -15) and mock transfectant control cells (Mock) were cultured and whole cell extracts (10 μg protein) were prepared and analyzed by immunoblotting with an antibody against each claudin or actin (A). These cells (2×10^5 (B) or 2×10^4 (C) cells/well) were cultured for 7 d (B) or 24 h (C) and samples were incubated with antibodies against each claudin and/or ZO-1 or occludin. After incubation with the respective secondary antibody, cells were inspected using fluorescence microscopy (B, C).

...ilization Among the claudins, we selected claudin-1, -2, ...-4 and -15 for study based on the fact that their expression has been linked to tumor progression, as well as the availability of their corresponding antibodies. We then examined the effect of overexpression of these claudins on both the intercellular barrier function of TJs, and on cell migration and invasion. This was achieved by constructing stable transfants of Caco-2 cells that continuously overexpress each claudin. As shown in Fig. 1A, we first confirmed the overexpression of each claudin by immunoblotting analysis.

We then examined the subcellular localization of the overexpressed claudins by immunostaining. As shown in Fig. 1B, all the claudins localized at the cell surface (see *XY* panels). Co-immunostaining assay for claudin and ZO-1 or occludin revealed good correspondence in their localization. Such localization was also observed in panels of the *XZ* (Fig. 1B). Such strong immunostaining for claudin was not observed in mock transfectant control cells (data not shown). The results presented in Fig. 1B suggest that each overexpressed claudin localizes at TJs.

We used cells at high density for experiments shown in Fig. 1B, as was also the case for the experiments illustrated in Fig. 2. However, as a lower density of cells (migrating and growing cells) is used in the invasion and migration assays (see Figs. 3 and 4), we also monitored the localization of each overexpressed claudin in cells cultured at low density. As shown in Fig. 1C, in this situation the claudins did not localize at the cell surface, but instead were found throughout the intracellular compartments. It therefore seems that the overexpressed claudins only gradually localized at the cell surface (TJs) in response to increasing cell density.

Effect of Overexpression of Claudins on the Barrier Function of TJs We examined the effect of overexpression of each claudin on the intercellular barrier function of TJs by

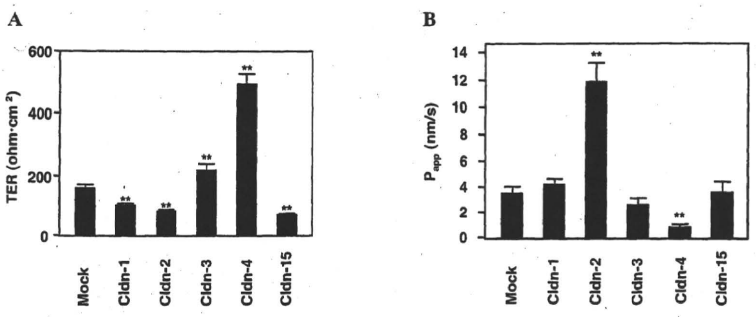

Fig. 2. Effect of Overexpression of Each Claudin on the Barrier Function of TJs

Caco-2 cells stably transfected with claudin-1, -2, -3, -4 or -15 expression plasmid (Cldn-1, -2, -3, -4 or -15) and mock transfectant control cells (Mock) were cultured for 7 d. The TER (A) and permeability of FD4 (B) were examined as described in Materials and Methods. Values are mean±S.D. (n=3). $^{**}p<0.01$ (A, B).

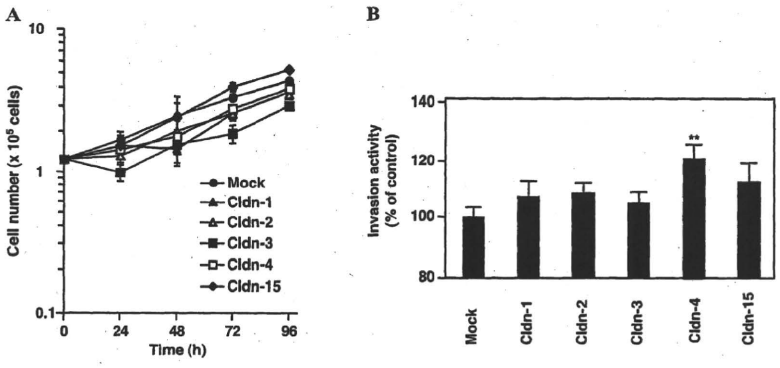

Fig. 3. Effect of Overexpression of Each Claudin on Cell Invasion

Caco-2 cells stably transfected with claudin-1, -2, -3, -4 or -15 expression plasmid (Cldn-1, -2, -3, -4 or -15) and mock transfectant control cells (Mock) were cultured for the indicated periods and cell numbers were determined by direct cell counting (A). These cells were cultured on matrigel-coated transwells for 48 h and invasion activity was measured as described in Materials and Methods. The results are expressed relative to the control (B). Values are mean±S.D. (n=3). $^{**}p<0.01$ (A, B).

examining the TER and permeability of FD4. TER is a measure of ion flux, mainly reflecting the ion flux across the TJs.[6] The TER in the mock transfectant control was 160 Ohm·cm^2 (Fig. 2A), which is similar to the value previously reported.[30] Overexpression of claudin-4 dramatically increased the TER, whereas overexpression of claudin-3 resulted in a similar but less pronounced effect (Fig. 2A). In contrast, overexpression of claudin-1, -2 and -15 produced a slight but significant decrease in the TER (Fig. 2A).

As shown in Fig. 2B, overexpression of claudin-4 or claudin-2 significantly decreased or increased, respectively, FD4 permeability, whereas overexpression of the other claudins had no significant effect (Fig. 2B). These results suggest that claudin overexpression can either positively or negatively affect the barrier function of TJs in Caco-2 cells, depending on the particular claudin species. In particular, overexpression of claudin-4 or claudin-2 seems to increase or decrease, respectively, the intercellular barrier function of TJs.

Effect of Overexpression of Claudins on Cell Invasion Figure 3A shows the growth curve of each clone. The growth of each of the claudin-overexpressing clones was indistinguishable from that of the mock transfectant control, demonstrating that the claudins did not affect the growth of the Caco-2 cells.

The effect of overexpression of each claudin on cell invasiveness was then examined using the transwell matrigel gel invasion assay. As shown in Fig. 3B, the claudin-4-overexpressing clone showed significantly greater cell invasion activity than the mock transfectant control. In contrast, clones overexpressing the other claudins produced similar results to the control (Fig. 3B), highlighting the specificity of the claudin-4 response.

Mechanism for Alteration of Cell Invasion Activity by Overexpression of Claudin-4 Cell migration is an important factor in determining cell invasiveness. We therefore examined the effect of overexpression of each claudin on cell migration, using the transwell chamber assay. As shown in Fig. 4A, claudin-2-overexpressing cells showed significantly greater cell migration activity than the mock transfectant control cells, whereas the claudin-3- or claudin-4-overexpressing cells showed less. These results reflect those previously observed in AGS cells.[21,22]

It has been reported that dynamic F-actin restructuring, in other words the formation of actin stress fibers, occurs in migrating cells and that this plays an important role in migration.[36] We used an immunostaining technique to examine the effect of overexpression of each claudin on F-actin architecture. A wound healing assay was used to obtain migrating cells, with the emergence of actin stress fibers being assessed 48 h after making the wound. As shown in Fig. 4B, typical actin stress fibers were observed in claudin-2-overexpressing cells. However, such a response was not observed in either the control cells or in those expressing the other claudins (Fig. 4B). These results suggest that overexpression of claudin-2 stimulates the formation of actin stress fibers, lead ing to the greater migration activity of these cells.

We next examined the localization of each overexpressed claudin in the wound healing cells. As shown in Fig. 4C (upper panel), not only claudin-2 but also the other claudins

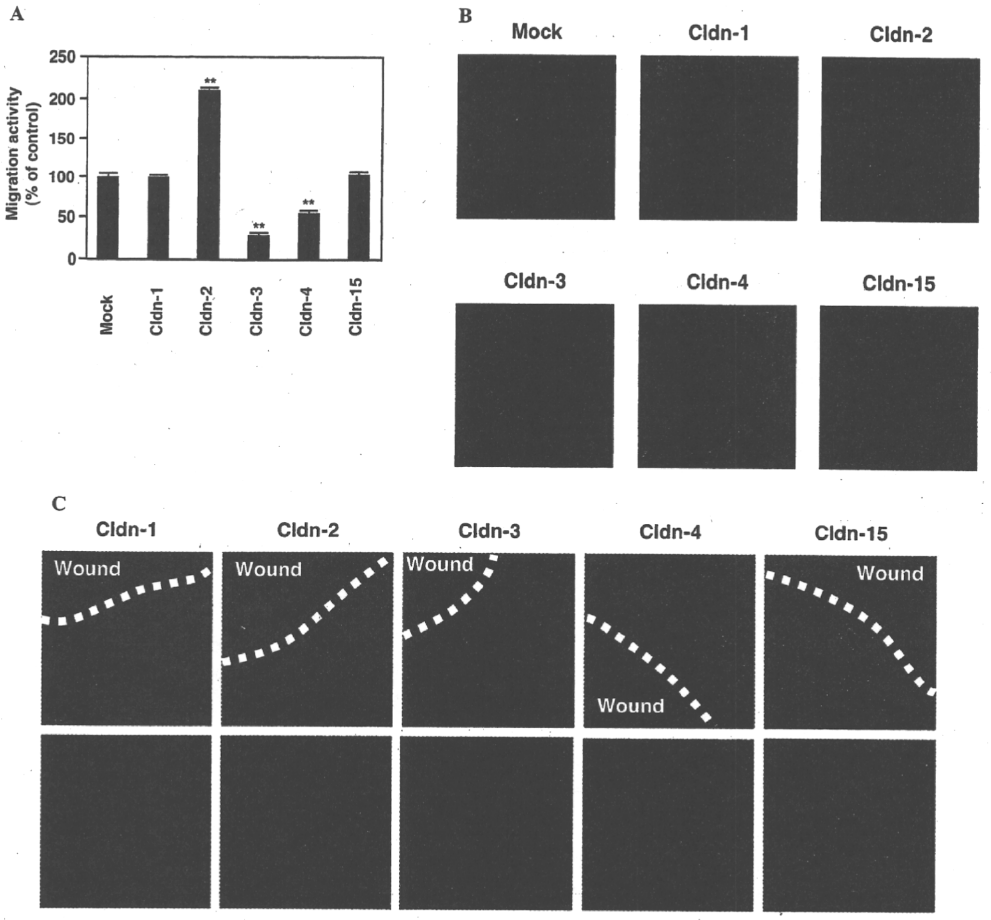

Fig. 4. Effect of Overexpression of Each Claudin on Cell Migration

Caco-2 cells stably transfected with claudin-1, -2, -3, -4 or -15 expression plasmid (Cldn-1, -2, -3, -4 or -15) and mock transfectant control cells (Mock) were cultured in transwell chambers for 48 h. Cell migration activity was measured as described in Materials and Methods and is expressed relative to the control. Values are mean±S.D. (n=3). $^{**}p<0.01$ (A). These cells were cultured for 7 d, then wounded, and cultured for a further 48 h (B, C). Actin stress fibers were observed by immunostaining (B). The localization of each claudin was monitored as described in the legend of Fig. 1. Wounded sides are shown by broken lines (C).

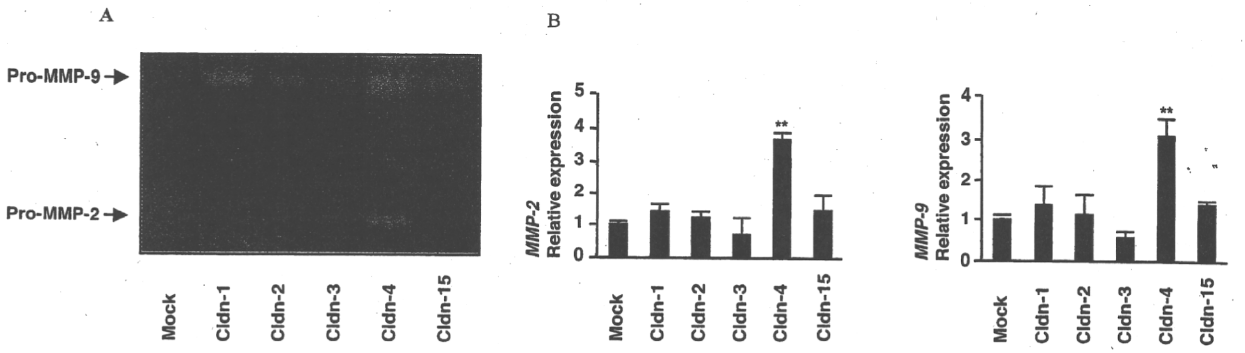

Fig. 5. Effect of Overexpression of Each Claudin on the Activity and Expression of MMPs

Caco-2 cells stably transfected with claudin-1, -2, -3, -4 or -15 expression plasmid (Cldn-1, -2, -3, -4 or -15) and mock transfectant control cells (Mock) were cultured for 24 h (A, B). MMP activity in the culture medium was measured as described in Materials and Methods (A). The mRNA expression of *MMP-2* and *MMP-9* was estimated by real-time RT-PCR as described in Materials and Methods. Values are mean±S.D. (n=3). $^{**}p<0.01$ (B).

were absent from the cell surface on the wounded side, but were present on the surface elsewhere. Distal to the wound, however, each of the claudins was found at the cell surface on all sides of the cell (Fig. 4C, lower panel). These results suggest that claudins generally translocate from the cell surface to the intracellular compartments at the site where cell migration occurs.

The results illustrated in Fig. 4A suggest that the higher invasive activity of cells expressing claudin-4 cannot be explained by its effect on cell migration. MMPs, especially MMP-2 and MMP-9, play an important role in cell invasion[37,38] and some claudins have been reported to modulate the activity of MMPs.[24,26] We therefore examined the effect of overexpression of each claudin on MMP-2 and MMP-9 activity using gelatin zymography. MMPs are proteolytically activated from pro-MMPs and both pro-MMPs and mature MMPs can be detected using this technique.[39] The band intensity of MMP-2, indicative of MMP-2 activity, was higher

in cells expressing claudin-4 than in mock transfectant control cells (Fig. 5A). Similar results were obtained for MMP-9 and pro-MMP-9 (Fig. 5A). In contrast, expression of the other claudins (claudin-1, -2, -3, -15) did not affect so clearly the intensity of these bands (Fig. 5A). These results suggest that the expression of claudin-4 specifically increases MMP-2 and MMP-9 activity, and that this may be responsible for the claudin-4-mediated stimulation of cell invasion.

Finally, mRNA expression of *MMP-2* and *MMP-9* in cells expressing each claudin was examined by real-time RT-PCR. As shown in Fig. 5B, the mRNA expression of both genes was up-regulated in cells expressing claudin-4 but not in those expressing the other claudins, suggesting that the higher activity of MMP-2 and MMP-9 in claudin-4-expressing cells is at least partly due to their higher expression.

DISCUSSION

Although it is generally believed that an alteration in claudin expression is involved in tumorigenesis, the role of individual claudins in the regulation of cancer-related cell functions, such as invasion and migration and regulating the intercellular barrier function of TJs, has remained unclear. This is because various types of cells, some of which lack the ability to form functional TJs, have been used in different studies. Therefore, in this study, we systematically examined the effect of overexpression of various claudins on Caco-2 cell invasion and migration, as well as on the intercellular barrier function of TJs, thereby allowing all these parameters to be investigated in a single system.

Overexpression of claudin-4 or claudin-2 either increased or deceased, respectively, TER in Caco-2 cells, results that are consistent with those obtained in other types of cells.[27,40,41] Overexpression of claudin-4 or claudin-2 also decreased or increased, respectively, the paracellular permeability of FD4 in these cells, suggesting that these claudins can exert an effect on cancer development by modulating the accessibility of nutrients and growth factors. As each of these claudins localizes at TJs under our experimental conditions, their differing effects on TJ barrier function appear to be due to their differing activities at these sites rather than differences in localization.

Overexpression of claudin-4, but not the other claudins, stimulated the invasive activity of Caco-2 cells. A similar effect has been observed in ovarian cancer cells (HOSE), whereas the opposite effect was observed in pancreatic cancer cells (SUIT-2).[16,25] Despite stimulating cell invasion, overexpression of claudin-4 inhibited the migration of Caco-2 cells, although it specifically increased the expression and activity of MMP-2 and MMP-9. Thus, MMP activity rather than cell migration appears to represent the mode of action by which claudin-4 stimulates cell invasion. It is known that claudins affect cell physiology through recruiting signal transduction-related molecules at TJs.[42] Furthermore, claudin-1, -2, -3 and -5 have been suggested to recruit and activate pro-MMP-2.[26,43] However, since overexpressed claudin-4 exists ubiquitously in cells under our culture conditions, claudin-4 could be affecting the expression and activity of MMPs either directly or by modulating signal transduction in the cytoplasm. Supporting this notion, the co-localization of claudins with MMP-2 is not limited to TJs but is also observed in the cytoplasm.[43]

Overexpression of claudin-2 or claudin-3 and -4 stimulated or inhibited, respectively, the migration of Caco-2 cells. We also observed actin stress fibers in Caco-2 cells expressing claudin-2, and found that each of these claudins delocalized from the cell surface to intracellular compartments after wound formation (activation of migration activity), an event that has previously been reported only for claudin-3.[44] Thus, migration-stimulating signals induce delocalization of claudins into intracellular compartments, with some of these claudins having a positive effect on cell migration whereas some of others exert the opposite effect. At present, the mechanism by which the different claudins influence cell migration remains unclear.

In summary, the results of this study suggest that overexpression of claudin-2 stimulates cancer development by decreasing the intercellular barrier function of TJs and increasing cell migration. On the other hand, the overall effect of overexpression of claudin-4 on cancer development remains unclear, as it increases both the intercellular barrier function of TJs and cell invasion. Furthermore, we found that the subcellular localization of TJs differs between cells cultured at high density (cells contacting each other) and those grown at low density (migrating and growing cells). Thus, it seems that claudin expression affects the invasion and migration activities and the intercellular barrier function of TJs independently, with both effects being important for cancer development.

Acknowledgements Grants-in-Aid of Scientific Research from the Ministry of Health, Labour, and Welfare of Japan, Grants-in-Aid for Scientific Research from the Ministry of Education, Culture, Sports, Science and Technology of Japan, and Grants-in-Aid of the Japan Science and Technology Agency.

REFERENCES

1) Hamazaki Y., Itoh M., Sasaki H., Furuse M., Tsukita S., *J. Biol. Chem.*, **277**, 455—461 (2002).
2) Itoh M., Furuse M., Morita K., Kubota K., Saitou M., Tsukita S., *J. Cell Biol.*, **147**, 1351—1363 (1999).
3) Anderson J. M., Van Itallie C. M., *Am. J. Physiol.*, **269**, G467—G475 (1995).
4) Tsukita S., Furuse M., Itoh M., *Nat. Rev. Mol. Cell Biol.*, **2**, 285—293 (2001).
5) Gonzalez-Mariscal L., Betanzos A., Nava P., Jaramillo B. E., *Prog. Biophys. Mol. Biol.*, **81**, 1—44 (2003).
6) Van Itallie C. M., Anderson J. M., *Annu. Rev. Physiol.*, **68**, 403—429 (2006).
7) Furuse M., Sasaki H., Fujimoto K., Tsukita S., *J. Cell Biol.*, **143**, 391—401 (1998).
8) Tsukita S., Furuse M., *J. Cell Biol.*, **149**, 13—16 (2000).
9) Morin P. J., *Cancer Res.*, **65**, 9603—9606 (2005).
10) Oliveira S. S., Morgado-Diaz J. A., *Cell. Mol. Life Sci.*, **64**, 17—28 (2007).
11) Swisshelm K., Macek R., Kubbies M., *Adv. Drug Deliv. Rev.*, **57**, 919—928 (2005).
12) Rangel L. B., Agarwal R., D'Souza T., Pizer E. S., Alo P. L., Lancaster W. D., Gregoire L., Schwartz D. R., Cho K. R., Morin P. J., *Clin. Cancer Res.*, **9**, 2567—2575 (2003).
13) Vermeer P. D., Einwalter L. A., Moninger T. O., Rokhlina T., Kern J. A., Zabner J., Welsh M. J., *Nature* (London), **422**, 322—326 (2003).
14) Soler A. P., Miller R. D., Laughlin K. V., Carp N. Z., Klurfeld D. M., Mullin J. M., *Carcinogenesis*, **20**, 1425—1431 (1999).
15) Nakajima M., Katayama K., Tamechika I., Hayashi K., Amano Y., Ue-

hata M., Goto N., Kondo T., *Clin. Exp. Pharmacol. Physiol.*, **30**, 457—463 (2003).
16) Michl P., Barth C., Buchholz M., Lerch M. M., Rolke M., Holzmann K. H., Menke A., Fensterer H., Giehl K., Lohr M., Leder G., Iwamura T., Adler G., Gress T. M., *Cancer Res.*, **63**, 6265—6271 (2003).
17) Miwa N., Furuse M., Tsukita S., Niikawa N., Nakamura Y., Furukawa Y., *Oncol. Res.*, **12**, 469—476 (2001).
18) Iacobuzio-Donahue C. A., Maitra A., Shen-Ong G. L., van Heek T., Ashfaq R., Meyer R., Walter K., Berg K., Hollingsworth M. A., Cameron J. L., Yeo C. J., Kern S. E., Goggins M., Hruban R. H., *Am. J. Pathol.*, **160**, 1239—1249 (2002).
19) Hough C. D., Sherman-Baust C. A., Pizer E. S., Montz F. J., Im D. D., Rosenshein N. B., Cho K. R., Riggins G. J., Morin P. J., *Cancer Res.*, **60**, 6281—6287 (2000).
20) Hewitt K. J., Agarwal R., Morin P. J., *BMC Cancer*, **6**, 186 (2006).
21) Mima S., Tsutsumi S., Ushijima H., Takeda M., Fukuda I., Yokomizo K., Suzuki K., Sano K., Nakanishi T., Tomisato W., Tsuchiya T., Mizushima T., *Cancer Res.*, **65**, 1868—1876 (2005).
22) Mima S., Takehara M., Takada H., Nishimura T., Hoshino T., Mizushima T., *Carcinogenesis*, **10**, 1994—2000 (2008).
23) Oku N., Sasabe E., Ueta E., Yamamoto T., Osaki T., *Cancer Res.*, **66**, 5251—5257 (2006).
24) Dhawan P., Singh A. B., Deane N. G., No Y., Shiou S. R., Schmidt C., Neff J., Washington M. K., Beauchamp R. D., *J. Clin. Invest.*, **115**, 1765—1776 (2005).
25) Agarwal R., D'Souza T., Morin P. J., *Cancer Res.*, **65**, 7378—7385 (2005).
26) Miyamori H., Takino T., Kobayashi Y., Tokai H., Itoh Y., Seiki M., Sato H., *J. Biol. Chem.*, **276**, 28204—28211 (2001).
27) Van Itallie C. M., Fanning A. S., Anderson J. M., *Am. J. Physiol. Renal. Physiol.*, **285**, F1078—F1084 (2003).
28) Blackman B., Russell T., Nordeen S. K., Medina D., Neville M. C., *Breast Cancer Res.*, **7**, R248—R255 (2005).
29) Boireau S., Buchert M., Samuel M. S., Pannequin J., Ryan J. L., Choquet A., Chapuis H., Rebillard X., Avances C., Ernst M., Joubert D., Mottet N., Hollande F., *Carcinogenesis*, **28**, 246—258 (2007).
30) Tavelin S., Hashimoto K., Malkinson J., Lazorova L., Toth I., Artursson P., *Mol. Pharmacol.*, **64**, 1530—1540 (2003).
31) Corral R. S., Iniguez M. A., Duque J., Lopez-Perez R., Fresno M., *Oncogene*, **26**, 958—969 (2007).
32) Taraboletti G., Sonzogni L., Vergani V., Hosseini G., Ceruti R., Ghilardi C., Bastone A., Toschi E., Borsotti P., Scanziani E., Giavazzi R., Pepper M. S., Stetler-Stevenson W. G., Bani M. R., *Exp. Cell Res.*, **258**, 384—394 (2000).
33) Bradford M. M., *Anal. Biochem.*, **72**, 248—254 (1976).
34) Larkins T. L., Nowell M., Singh S., Sanford G. L., *BMC Cancer*, **6**, 181 (2006).
35) Biganzoli E., Cavenaghi L. A., Rossi R., Brunati M. C., Nolli M. L., *Farmaco*, **54**, 594—599 (1999).
36) Pellegrin S., Mellor H., *J. Cell Sci.*, **120**, 3491—3499 (2007).
37) Egeblad M., Werb Z., *Nat. Rev. Cancer*, **2**, 161—174 (2002).
38) Deryugina E. I., Quigley J. P., *Cancer Metastasis Rev.*, **25**, 9—34 (2006).
39) Fu X., Parks W. C., Heinecke J. W., *Semin. Cell Dev. Biol.*, **19**, 2—13 (2008).
40) Furuse M., Furuse K., Sasaki H., Tsukita S., *J. Cell Biol.*, **153**, 263—272 (2001).
41) Van Itallie C., Rahner C., Anderson J. M., *J. Clin. Invest.*, **107**, 1319—1327 (2001).
42) Matter K., Balda M. S., *Nat. Rev. Mol. Cell Biol.*, **4**, 225—236 (2003).
43) Ichiyasu H., McCormack J. M., McCarthy K. M., Dombkowski D., Preffer F. I., Schneeberger E. E., *Am. J. Respir. Cell Mol. Biol.*, **30**, 761—770 (2004).
44) Matsuda M., Kubo A., Furuse M., Tsukita S., *J. Cell Sci.*, **117**, 1247—1257 (2004).

Pharmaceutical Research, Vol. 26, No. 7, July 2009 (© 2009)
DOI: 10.1007/s11095-009-9891-5

Research Paper

Synthesis of Prostaglandin E_1 Phosphate Derivatives and Their Encapsulation in Biodegradable Nanoparticles

Miho Takeda,[1] Taishi Maeda,[1] Tsutomu Ishihara,[1,2] Haruka Sakamoto,[1] Kanae Yuki,[1] Naoko Takasaki,[1] Fumihiro Nishimura,[1] Takeshi Yamashita,[1] Ken-ichiro Tanaka,[1] Mitsuko Takenaga,[3] Rie Igarashi,[3] Megumu Higaki,[2] Naoki Yamakawa,[1] Yoshinari Okamoto,[1] Hisao Ogawa,[1] Masami Otsuka,[1] Yutaka Mizushima,[2] and Tohru Mizushima[1,4]

Received December 25, 2008; accepted April 5, 2009; published online May 5, 2009

Purpose. Prostaglandin E_1 (PGE_1) is an effective treatment for peripheral vascular diseases. The encapsulation of PGE_1 in nanoparticles for its sustained-release would improve its therapeutic effect and quality of life (QOL) of patients.
Methods. In order to encapsulate PGE_1 in nanoparticles prepared with a poly(lactide) homopolymer (PLA) and monomethoxy poly(ethyleneglycol)-PLA block copolymer (PEG-PLA), we synthesized a series of PGE_1 phosphate derivatives and tested their efficacy.
Results. Among them, PGE_1 2-(phosphonooxy)ethyl ester sodium salt (C2) showed the most efficient hydrolysis to yield PGE_1 in human serum. An *in vitro* platelet aggregation assay showed that C2 inhibited aggregation only after pre-incubation in serum, suggesting that C2 is a prodrug of PGE_1. *In vivo*, intravenous administration of C2 caused increase in cutaneous blood flow. In the presence of zinc ions, all of the synthesized PGE_1 phosphate derivatives could be encapsulated in PLA-nanoparticles. Use of L-PLA instead of D,L-PLA, and high molecular weight PLA resulted in a slower release of C2 from the nanoparticles.
Conclusions. We consider that C2-encapsulated nanoparticles prepared with L-PLA and PEG-D,L-PLA have good sustained-release profile of PGE_1, which is useful clinically.

KEY WORDS: biodegradable nanoparticles; encapsulation; prostaglandin E_1; zinc.

Miho Takeda and Taishi Maeda equally contribute to this work.

Electronic supplementary material The online version of this article (doi:10.1007/s11095-009-9891-5) contains supplementary material, which is available to authorized users.

[1] Graduate School of Medical and Pharmaceutical Sciences, Kumamoto University, 5-1 Oe-honmachi, Kumamoto 862-0973, Japan.
[2] DDS Institute, The Jikei University School of Medicine, Tokyo 105-8461, Japan.
[3] Division of Drug Delivery System, Institute of Medical Science, St. Marianna University, Kawasaki 216-8512, Japan.
[4] To whom correspondence should be addressed. (e-mail: mizu@gpo.kumamoto-u.ac.jp)

ABBREVIATIONS: ADAM, 9-anthryldiazomethane; ADP, adenosine 5′-diphosphate; ALP, alkaline phosphatase; AS-013, Δ^8-9-*O*-butyryl prostaglandin F_1 butyl ester; $(BnO)_2$-PN$(CH(CH_3)_2)_2$, dibenzyl *N*,*N*-diisopropyl phosphoramidite; C*x* (x=2, 3, 4, 6, 12), PGE_1 *x*-(phosphonooxy)alkyl ester sodium salt; DEA, diethanolamine; DMAP, 4-dimethylaminopyridine; EDC, 1-ethyl-3-(3-dimethylaminopropyl) carbodiimide hydrochloride; EtOAc, ethyl acetate; FAB, fast atom bombardment; EPR, enhanced permeability and retention; HCl, hydrochloric acid; ^{1}H-NMR, proton nuclear magnetic resonance; HPLC, high-performance liquid chromatography; *m*-CPBA, *m*-chloroperoxybenzoic acid; MPS, mononuclear phagocyte system; MQW, Milli-Q water; MS, mass spectra; Mw, molecular weight; PBS, phosphate-buffered saline; PEG, poly(ethyleneglycol)PGE1, prostaglandin E1; PLA, poly(lactide); PLE, porcine liver esterase; PPP, platelet-poor plasma; PRP, platelet-rich plasma; QOL, quality of life; S.E.M., standard error mean; Tris, tris(hydroxymethyl) aminomethane.

INTRODUCTION

The number of patients with peripheral obstructive vascular diseases such as arteriosclerosis obliterans has increased in line with aging of the population and increases in the prevalence of diabetes and hyperlipidemia. The condition can result in amputation of lower limbs or even death in severely affected patients (1). Various clinical treatments such as vascular bypass surgery have been developed for these diseases; however, the prognosis is not still good. Furthermore, a large number of patients (about 5–8% of elderly) suffer from mild peripheral vascular diseases (such as intermittent claudication) (2), for which effective drug treatments have not been established.

Prostaglandin E_1 (PGE_1), which has various physiological actions such as vasodilation, angiogenesis and inhibition of platelet aggregation, may thus serve as an effective treatment for peripheral obstructive vascular diseases. Results from a number of clinical and animal studies support this notion (3–5). However, the range of activities of PGE_1 are also related to adverse effects (such as hypotension and diarrhea) due to its distribution throughout the body when administered systemically (4,6). Furthermore, in addition to its chemical instability (hydrolysis to PGA_1), PGE_1 is easily inactivated by 15-hydroxydehydrogenase during the passage through the lung (7–9). Therefore, a drug delivery system that enables the stabilization of PGE_1 and its targeting at the site

of vascular injury is important. With these points in mind, we developed lipo-PGE_1, a preparation incorporating PGE_1 into an oil-in-water lipid emulsion (lipid microspheres) consisting of a soybean oil core and lecithin surfactant with a diameter of approximately 200 nm (10–12). Incorporation of PGE_1 into lipid microspheres protects PGE_1 from inactivation in the lung and enables the selective delivery of PGE_1 to damaged blood vessels, resulting in enhanced therapeutic effects and reduced adverse effects (10,13,14). Lipo-PGE_1 is used clinically in Japan, South Korea and China for systemic administration and exhibits a more potent therapeutic effect for peripheral obstructive vascular diseases than does PGE_1 clathrated in cyclodextrin which is used clinically worldwide (12,15). We also synthesized a stable PGE_1 prodrug (Δ^8-9-*O*-butyryl prostaglandin F_1 butyl ester, AS-013) and lipo-AS-013 showed superior characteristics to lipo-PGE_1 in both animal and clinical studies (6,16,17). However, lipid microspheres cannot retain PGE_1 for a long period of time *in vivo* (16,18). Therefore, daily intravenous drip infusion is necessary for clinical treatment with lipo-PGE_1, which in turn requires patient hospitalization, resulting in a low quality of life (QOL). Encapsulation of PGE_1 in more stable nanoparticles that permit a longer-lasting therapeutic effect provided by the sustained-release of PGE_1 would consequently be of significant clinical benefit. Encapsulation of PGE_1 in nanoparticles with size of approximately 50–200 nm would enhance the selective delivery of PGE_1 to damaged blood vessels due to the enhanced permeability and retention (EPR) effect (14).

The encapsulation of drugs in biodegradable and biocompatible polymeric solid particles, such as poly(lactide) homopolymer (PLA)-particles is effective for achieving a sustained-release formulation of drugs (19–21). For example, encapsulation of luteinizing hormone-releasing hormone in microparticles prepared from PLA achieved a long-term therapeutic effect by enabling sustained-release of the hormone concomitant with the degradation of PLA, as has already been employed in clinical practice (22,23). Thus, PLA-nanoparticles (diameter 50–200 nm for the EPR effect) with sustained-release of PGE_1 may prove beneficial for the treatment of peripheral obstructive vascular diseases. One obstacle to the use of solid nanoparticles in the treatment of patients in clinical practice is the uptake of these particles by the mononuclear phagocyte system (MPS), or in other words by the reticuloendothelial system (21,24). Use of a monomethoxy poly (ethyleneglycol)-PLA block copolymer (PEG-PLA) enables the nanoparticles to escape from this uptake due to the steric barrier by which the PEG chain prevents interaction of the nanoparticles with opsonins and cells responsible for MPS, such as Kupffer cells (stealth effect) (18,21,24). Another obstacle is that relatively hydrophilic drugs, such as PGE_1 and betamethasone, are very hard to encapsulate in PLA-nanoparticles (25–27). Hydrophilic drugs can be encapsulated into nanoparticles using a double emulsion (*w/o/w*) process, however, the size of this type of particles is generally more than 400 nm diameter and may have less EPR effect. For betamethasone, we recently overcame this obstacle by using betamethasone phosphate. After insolubilization in the presence of zinc, betamethasone phosphate could be efficiently encapsulated in PLA-nanoparticles by the oil-in-water solvent diffusion method. Betamethasone phosphate released upon degradation of the nanoparticles could then be hydrolyzed to yield betamethasone both *in vitro* and *in vivo*; resulting in a long-lasting therapeutic effect (28,29).

In the present study, we synthesized a series of PGE_1 phosphate derivatives with different spacer (alkyl chain) length (PGE_1 *x*-(phosphonooxy)alkyl ester sodium salt (C*x*; x=2, 3, 4, 6, 12)) and evaluated their efficacy both *in vitro* and *in vivo*. All of these derivatives can be encapsulated in PLA-nanoparticles. Of the derivatives, C2 showed the most efficient hydrolysis to yield PGE_1 in human serum. C2 showed a potent inhibitory activity on platelet aggregation *in vitro* and increased cutaneous blood flow *in vivo*. C2-encapsulated nanoparticles prepared with L-PLA and PEG-D,L-PLA showed a good sustained-release profile of C2.

MATERIALS AND METHODS

Materials and Animals

D,L-PLA, zinc chloride and 1,4-dioxane were purchased from Wako Pure Chemicals Industries, Ltd. (Osaka, Japan). L-PLA was from Taki Chemical Co., Ltd. (Kakogawa, Japan). AS-013 was from our laboratory stock. PEG-D,L-PLA (average molecular weight of PEG and PLA are 5,600 and 9,400, respectively) was synthesized and evaluated as described previously (18,30). Porcine liver esterase (PLE) and human placenta alkaline phosphatase (ALP) were purchased from Sigma-Aldrich Co. (St. Louis, MO). Wistar rats (6 weeks old, male) were from Kyudo Co., Ltd. (Kumamoto, Japan). The experiments and procedures described here were carried out in accordance with the Guide for the Care and Use of Laboratory Animals as adopted and promulgated by the National Institute of Health, and were approved by the Animal Care Committee of Kumamoto University.

Analysis of Synthesized Molecules

Low-resolution- and high-resolution-fast atom bombardment (FAB) mass spectra (MS) were measured on a JMS-700 instrument (JEOL Ltd., Tokyo, Japan). Proton nuclear magnetic resonance (^{1}H-NMR) spectra were recorded on a JNM AL-300 instrument (300 MHz) (JEOL Ltd., Tokyo, Japan), using tetramethylsilane as an internal standard. Analytical thin-layer chromatography was performed using silica gel glass plates (60 F_{254}) (Merck Ltd., Tokyo, Japan). Column chromatography was performed using Silica gel 60N (Kanto Chemical Co., Tokyo, Japan). Compound 4 (PE1) shown in Fig. 1 was obtained from Daiichi Fine Chemical Co., Ltd. (Takaoka, Japan)

Synthesis of PGE_1 Phosphate

The structures of PGE_1 phosphate derivatives and outlines of their synthesis are shown in Fig. 1. The recovery of each compound and analysis of NMR data are provided in the supplementary information.

Compounds (1a–e) (1.7 mmol) were mixed with 1*H*-tetrazole (2.5 mmol) and dibenzyl *N,N*-diisopropyl phosphoramidite ($(BnO)_2$-$PN(CH(CH_3)_2)_2$) (3.4 mmol) in dichloromethane (10 ml). After stirring at room temperature overnight, *m*-chloroperoxybenzoic acid (*m*-CPBA) (3.4 mmol)

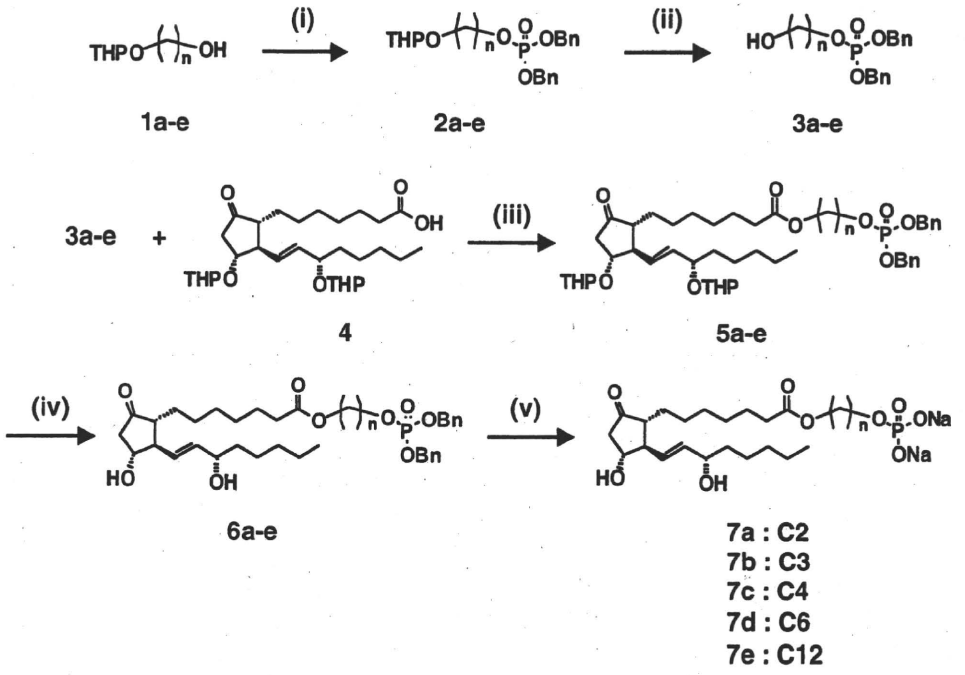

Fig. 1. Pathways for the synthesis of PGE_1 phosphate derivatives. Compounds: 1a–3a, 5a–7a (n=2); 1b–3b, 5b–7b (n=3); 1c–3c, 5c–7c (n=4); 1d–3d, 5d–7d (n=6); 1e–3e, 5e–7e (n=12). Reagents and solvents: *(i)* $(BnO)_2$-PN($CH(CH_3)_2)_2$, 1*H*-tetrazole, *m*-CPBA, dichloromethane; *(ii)* pyridinium *p*-toluene sulfonate, ethanol; *(iii)* EDC, DMAP, dichloromethane; *(iv)* acetic acid, tetrahydrofuran, MQW; *(v)* 1,4-cyclohexadiene, 10% palladium-carbon, acetic acid, sodium acetate, ethanol.

was added and stirred at room temperature for 30 min. The mixture was diluted with chloroform (30 ml), washed successively with saturated sodium hydrogen carbonate (10 ml×3) and saturated sodium chloride (10 ml×3). The organic layer was dried over sodium sulfate and concentrated in vacuo. The resulting residue was purified by silica gel column chromatography (from ethyl acetate (EtOAc)/hexane=1:1 to 100% EtOAc) to give compounds (2a–e) as a colourless oil.

Compounds (2a–e) (1.35 mmol) and pyridinium *p*-toluene sulfonate (0.3 mmol) in ethanol (5 ml) were stirred at 55°C for 3 h. After evaporation, the residue was purified by silica gel column chromatography (from EtOAc/hexane=3:2 to 100% EtOAc) to give compounds (3a–e) as a colourless oil.

Compounds (3a–e) (0.25 mmol), 1-ethyl-3-(3-dimethylaminopropyl) carbodiimide hydrochloride (EDC) (0.4 mmol), 4-dimethylaminopyridine (DMAP) (0.2 mmol) and compound 4 (PE1) (0.2 mmol) in dichloromethane (3 ml) were stirred at room temperature for 10 min. The mixture was diluted with chloroform (30 ml) and washed successively with saturated sodium hydrogen carbonate (10 ml×3) and saturated sodium chloride (10 ml×3). The organic layer was dried over sodium sulfate and concentrated in vacuo. The residue was purified by silica gel column chromatography (EtOAc/hexane=1:1) to give compounds (5a–e) as a colourless oil.

Compounds (5a–e) (0.052 mmol) in acetic acid (1.8 ml)/tetrahydrofuran (0.45 ml)/Milli-Q water (MQW) (1.8 ml) were stirred at 35°C for 4 h and mixed with saturated sodium hydrogen carbonate (5 ml) at 0°C. The mixture was extracted with EtOAc (50 ml×3) and the combined organic layer was washed with saturated sodium chloride (10 ml×3) and dried over sodium sulfate and concentrated in vacuo. The residue was purified by silica gel column chromatography (from EtOAc/hexane=1:1 to 100% EtOAc) to give compounds (6a–e) as a colourless oil.

Compounds (6a–e) (0.026 mmol) were mixed with 10% palladium-carbon (64 mg) in 1,4-cyclohexadiene (2.8 ml)/acetic acid (0.2 ml)/ethanol (5 ml). After stirring at room temperature for 2 h, sodium acetate (0.052 mmol) was added and 10% palladium-carbon was removed by filtration, followed by washing with ethanol. The combined filtrate was concentrated to give compounds (7a–e) as a yellowish paste.

Determination of PGE_1 and Its Derivatives

A Waters Alliance system, running Empower software (Milford, MA), was used for the high-performance liquid chromatography (HPLC) analysis. Samples were separated using a 4.6×100-mm TSKgel Super-ODS column (Tosoh Co., Tokyo, Japan).

For detection of PGE_1 phosphate derivatives, solvent A (acetonitrile) and solvent B (5 mM ammonium acetate) were used at a flow rate of 0.5 ml/min. After injection of sample (0 min), the mobile phase was changed as follows; 25% solvent A (1 min), a linear gradient of 25–60% solvent A (7 min), a linear gradient of 60–100% solvent A (5 min) and 100% solvent A (7 min). The detection was performed at 195 nm.

For detection of PGE_1, solvent A (acetonitrile) and solvent B (MQW) were used at a flow rate of 0.3 ml/min. Samples were incubated with 9-anthryldiazomethane (ADAM) (Funakoshi Co. Ltd., Tokyo, Japan) at 37°C for 8 h. After injection of the sample (0 min), the mobile phase was changed as follows; 65% solvent A (25 min), a linear gradient of 65–100% solvent A

(10 min) and 100% solvent A (10 min). Fluorescence at 412 nm (fluorescence peak wavelength of ADAM reagent) was detected using a 2475 Multi λ Fluorescence Detector.

Preparation and Characterization of Nanoparticles

Nanoparticles were prepared by the oil-in-water solvent diffusion method as described previously (30). L-PLA in 1,4-dioxane or D,L-PLA in acetone was mixed with PEG-D,L-PLA and diethanolamine (DEA) in acetone and zinc chloride and each PGE_1 phosphate derivative in MQW (the total amount of block copolymers and homopolymer was fixed at 25 mg and total volume was 0.8 ml). Samples were incubated for 10 min at room temperature. The mixture was added dropwise (at a rate of 48 ml/h) to 25 ml of MQW stirred at 1,000 rpm. After addition of 0.5 ml of 0.5 M sodium citrate (pH 7.0) and 12.5 μl of 200 mg/ml Tween80, nanoparticles were purified and concentrated by ultrafiltration (Centriprep YM-50, Millipore Co., Billerica, MA).

For determination of the PGE_1 phosphate derivative content in nanoparticles, the nanoparticle suspension was mixed with 0.01 M sodium citrate (pH 7.0) and centrifuged at 50,000×*g* for 30 min. The pellet was washed and suspended in MQW, freeze-dried and weighed. The PGE_1 phosphate derivative content was determined using HPLC, as described above. The drug content was defined as the ratio of PGE_1 phosphate derivative weight to the total weight of nanoparticles.

Particle size and distribution were determined by the dynamic light scattering method (ZETASIZER Nano-ZS, Malvern Instruments Ltd., Malvern, UK) and the average diameter was calculated by Marquadt's method.

Treatment of PGE_1 Phosphate Derivatives with Serum, Plasma and Enzyme

This assay was performed as described in (16) with some modifications. The PGE_1 phosphate derivative (1 mM) was incubated at 37°C in 0.1 ml of human serum, rat plasma, or 0.1 M tris(hydroxymethyl) aminomethane (Tris)/hydrochloric acid (HCl) (pH 7.4) containing 2.5 U PLE or 25 mU ALP. Samples were taken periodically and diluted with ice-cold methanol. After incubation on ice for 30 min, the mixtures were centrifuged at 16,100×*g* for 10 min. The supernatants were evaporated to dryness and PGE_1 or its derivative content was determined by HPLC as described above.

Assay of Inhibition of Platelet Aggregation

This assay was performed as described in (17) with some modifications. Venous blood was collected from healthy human volunteers using 3.8% sodium citrate as an anticoagulant. Samples were centrifuged for 15 min at 160×*g* to obtain the upper phase (platelet-rich plasma (PRP)), and the lower phase was further centrifuged for 10 min at 1,500×*g* to obtain platelet-poor plasma (PPP). PRP was pre-incubated with PGE_1 or its derivatives and then mixed with adenosine 5′-diphosphate (ADP) (2 μM at final concentration). Samples were further incubated for 3 min and the extent of aggregation was measured using an NKK hematracer (PAC-8S, Niko Bioscience Co., Ltd., Tokyo, Japan). PPP was used as control.

Measurement of Cutaneous Blood Flow

This was performed as described in (17) with some modifications. Wistar rats were anaesthetized and a blood flow meter probe (ALF21, Advance Co., Osaka, Japan) was attached to left planta pedis. PGE_1 or C2 was intravenously administered via the tail vein at a dose of 10 nmol/kg.

RESULTS

The structures of PGE_1 phosphate derivatives and outlines of their synthesis are shown in Fig. 1. Tetrahydropyran ethers (1a–e) (31) were reacted with $(BnO)_2$-$PN(CH(CH_3)_2)_2$ in the presence of 1*H*-tetrazole to give dibenzyl phosphites, which were then oxidized with *m*-CPBA to yield dibenzyl phosphates (2a–e). The tetrahydropyran-protected group of 2a–e was deblocked by treatment with pyridinium *p*-toluene sulfonate in ethanol to afford alcohols (3a–e). These alcohols were then coupled to compound 4 (PE1), producing esters (5a–e). Removal of the tetrahydropyran-protected groups in 5a–e with aqueous acetic acid gave 6a–e. Catalytic hydrogenation with 1,4-cyclohexadiene of 6a–e was followed by treatment with sodium acetate to provide the desired sodium salts (7a–e).

We prepared Cn (n=2, 3, 4, 6, 12)-encapsulated nanoparticles with D,L-PLA, PEG-D,L-PLA, zinc chloride and DEA by the solvent diffusion method using the same protocol as that used for preparation of betamethasone phosphate-encapsulated PLA-nanoparticles (30). The particle size was similar for the different PGE_1 phosphate derivatives (Fig. 2A). On the other hand, the efficiency of encapsulation (drug content of nanoparticles) increased as a function of the spacer (alkyl chain) length (Fig. 2B). As was the case for betamethasone phosphate, very little of each PGE_1 phosphate derivative (less than 0.1%) could be encapsulated in the nanoparticles prepared in the absence of zinc chloride, and PGE_1 could not be encapsulated in the nanoparticles even in the presence of zinc chloride (data not shown), suggesting that insolubilization due to the interaction between zinc ion and phosphate group is important for efficient encapsulation. These PEG-containing nanoparticles seem to have a "core-corona" structure, because the zeta potential value was much lower than that of PEG-non-containing nanoparticles (deta not shown).

The efficiency of each PGE_1 phosphate derivative for hydrolysis by PLE or ALP was compared. As shown in Fig. 3A, in addition to AS-013, the compounds C6 and C12 were gradually hydrolyzed to yield PGE_1 in the presence of PLE, while C2, C3 and C4 were not. On the other hand, all of the PGE_1 phosphate derivatives tested were hydrolyzed by ALP, although the efficiency was different for each one (Fig. 3B). We also compared the production of PGE_1 from each PGE_1 phosphate derivative in human serum. As shown in Fig. 3C, a clear-cut production was observed only with AS-013 and C2. Based on results in Fig. 3A–C, we hypothesized that C2 can be hydrolyzed by esterase if the phosphate group is removed by phosphatase. To test this notion, we examined the production of PGE_1 from C2 in the presence of both PLE and ALP. The efficient production of PGE_1 was observed in the presence of both enzymes, but not with PLE or ALP alone (Fig. 3A, D). We also examined the production of PGE_1 from C2 in rat plasma and found that this took place